Effective separation of toxic azo dyes from water system using the activated carbon derived from *Prosopis juliflora* roots

J. Oliver Paul Nayagam[a], K. Prasanna[a,*], P. Senthil Kumar[b,c,d,e]

[a]*Department of Civil Engineering, SRM Institute Science and Technology, SRM Nagar, Kattankulathur, Kanchipuram – 603 203, Tamil Nadu, India, emails: prasannk@srmist.edu.in (K. Prasanna), oj1145@srmist.edu.in (J. Oliver Paul Nayagam)*
[b]*Department of Chemical Engineering, Sri Sivasubramaniya Nadar College of Engineering, Chennai – 603110, India, emails: senthilkumarp@ssn.edu.in*
[c]*Centre of Excellence in Water Research (CEWAR) Sri Sivasubramaniya Nadar College of Engineering, Chennai – 603110, India*
[d]*School of Engineering, Lebanese American University, Byblos, Lebanon*
[e]*Department of Biotechnology Engineering and Food Technology, Chandigarh University, Mohali – 140413, India*

ABSTRACT

An experimental investigation of azo dye removal using activated *Prosopis juliflora* root was carried out using the batch adsorption technique. The *P. juliflora* roots were collected and synthesized using a chemical synthesis technique, and their pore size and surface area was analyzed using N_2 – adsorption and desorption process. The scanning electron microscopy/energy-dispersive X-ray spectroscopy analysis confirms the presence of targeted azo dyes on the surface of the prepared adsorbent material and the thermal stability of the adsorbent was analyzed using thermogravimetric analysis and derivative thermogravimetry. The X-ray diffraction analysis shows the amorphous structure and the intensity of activated charcoal *P. juliflora* adsorbent. Batch adsorption studies were conducted to determine the optimal adsorption parameters such as pH, dosage level, concentrations, contact time, and temperature. Adsorption kinetic studies confirm the favorable adsorption process between the adsorbate and the adsorbent, and isotherm studies fitted well with the high regression values. Thermodynamic studies revealed the adsorption between the adsorbent and adsorbate to be endothermic, and the desorption studies confirmed the high recovery of spent adsorbent using concentrated sulphuric acid. As a result, the activated *P. juliflora* powder adsorbs 99.6% of Reactive Orange – RO-16, 94.43% of Reactive Red – RR-120, and 82.26% of Reactive Blue – RB-19 azo dyes from the prepared synthetic solutions in batch mode of adsorption process.

Keywords: Prosopis juliflora roots adsorbent; Synthetic dye removal; Isothermal studies; Thermodynamic studies; Kinetic modelling

1. Introduction

From the environmental perspective, pollution from the industries has been increasingly creating severe problems for all living beings. Various pollutants have been identified from the industrial activities, amongst which, water pollution is of significant concern because of the need for water for all surviving organisms. Water gets polluted due to the increasing release of a number of toxic pollutants like heavy metals, dyes, inorganic compounds, suspended and dissolved solids, etc., [1]. Industries release effluents containing all these pollutants without any prior treatment because of the very high cost and maintenance entailed [2]. Textile industries is one of the many sources that create toxic effects on the environment because of the presence of inorganic pollutants. Compared to all industries, the textile

* Corresponding author.

manufacturing units release excess wastewater into the water bodies [3]. The industries generate 45–60 L of wastewater for 1 kg of material production [4]. These untreated textile industry effluents contain reactive/synthetic dyes which are highly visible as different colours [5]. These dyes were identified as the most toxic of materials, quickly reacting with the soluble functional groups in the water and creating water-borne diseases, nausea, skin ulceration, etc., [6]. Dyes may be classified as reactive and acid type, primary cationic type, and disperse non-ionic type. The basic dyes have very high visibility and intensity even at low concentrations, and these are identified as toxic and severe problem-creating compounds [7–11].

Conventional methods such as ion exchange, membrane filtration, adsorption, biological treatment, etc., reduce and remove the concentration and colour intensity from the aqueous solutions. The main problems with adopting these technologies are high investment and maintenance costs, generation of by-products, and dioxin formation [12]. Due to these kinds of issues, the industries failed to adopt these technologies and released the raw effluent into the water bodies [10]. However, the need of the hour is the use of suitable technology to control the water pollution because of dyes [13]. Hence it was decided to use the biosorption process to reduce the concentration and intensity of synthetic dyes from the wastewater. The process of adsorption is nothing but the adhesion of pollutants from any medium onto the surface of the adsorbent material due to forces of attraction [14]. This method has several advantages like selective removal of materials, low investment, and high efficiency [15]. Nowadays, organic and inorganic materials such as date seeds, fly ash, neem leaves, grape peels, etc., are used as adsorbent materials using chemical activation process, which provides exceptionally high efficiency for the adsorption process [16]. Here, the *Prosopis juliflora* activated carbon was used to remove the reactive dyes from the prepared synthetic solutions by batch adsorption study. Various activated carbons were used commercially to remove the

pollutants from aqueous solutions [17]. *P. juliflora* is a small tree used as firewood introduced in 1877 in India [18]. The roots of even a small tree can penetrate to a depth of 60 m and consume more groundwater. The distribution of *P. juliflora* trees in the world and India are seen in Fig. 1.

Excessive accumulation of these trees may consume more groundwater and create severe problems for the surrounding environment [19]. In Tamil Nadu, Ramanathapuram is a district with a significant accumulation of *P. juliflora* trees, reducing the groundwater table for entire rural and urban areas [20]. Hence, it was decided to use these trees as an adsorptive material to remove synthetic dyes from the aqueous solutions. In this research work, the *P. juliflora* tree was used as an adsorbent material for removing Reactive Orange – RO-16, Reactive Red – RR-120 and Reactive Blue – RB-19 dyes from the synthetic solutions. The chemical composition of azo dyes (RO-16, RR-120 and RB-19) is shown in Fig. 2. The batch mode of adsorption study was conducted under various operating conditions, and the kinetic and thermodynamic studies were conducted to evaluate the process of adsorption. The biochar was obtained from the *P. juliflora* roots, and used as an adsorbent material for removing the various dyes from the aqueous solutions.

2. Materials and methods

2.1. Adsorbent preparation

The *P. juliflora* plants were collected from the Ramanathapuram district in Tamil Nadu, India, and the leaves and branches were completely removed/ The roots were sun-dried and washed several times to remove all impurities. The root samples were then cut into small pieces (2–3 cm in size) and ground into fine powder by a mechanical synthesis process [21]. The finely ground powder was taken and placed in the muffle furnace and heated at 400°C to prepare the charcoal, powder for the experimental analysis. The samples were next taken from the furnace and
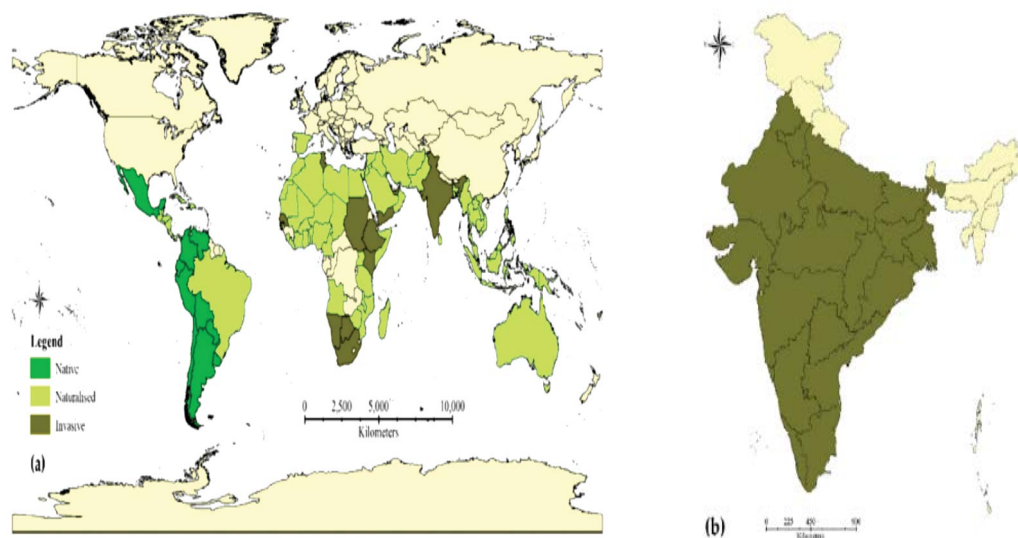

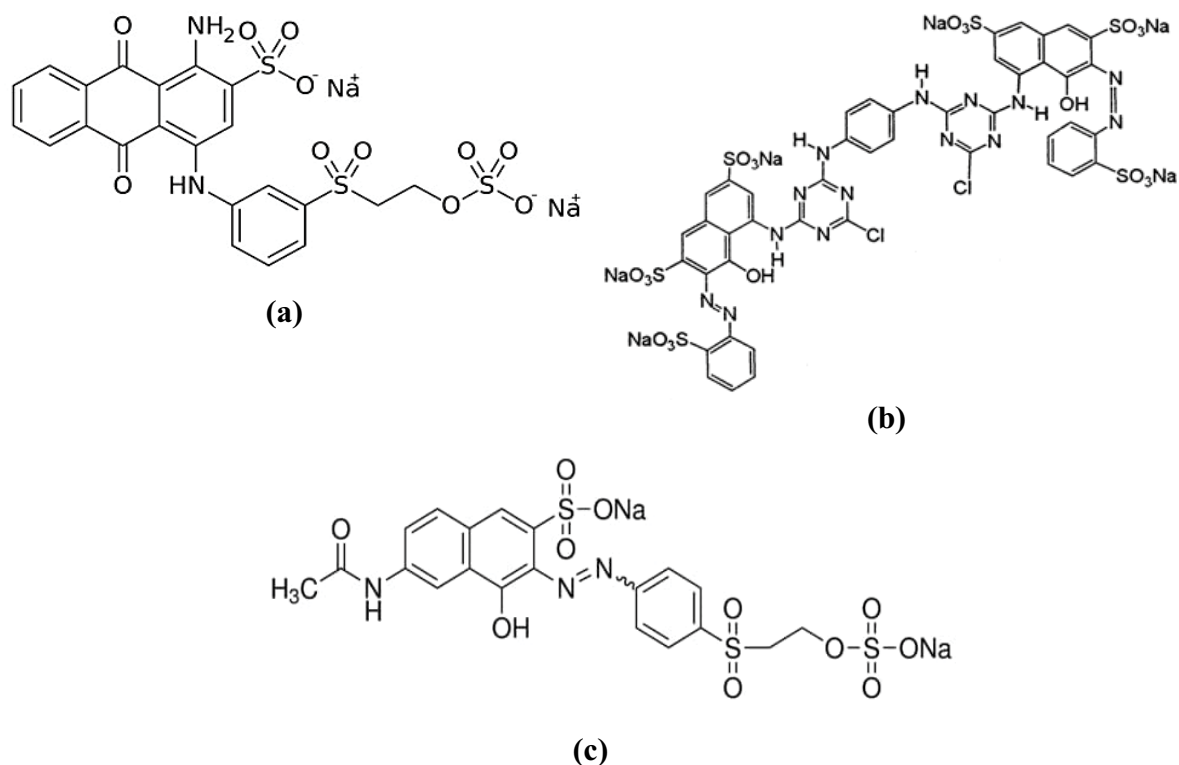Fig. 1. Availability of *Prosopis juliflora* trees in and around the world.

Fig. 2. Chemical composition of (a) RO-16, (b) RR-120 and (c) RB-19 azo dyes.

washed with double distilled water to completely eliminate the impurities and toxins. The charcoal powder was then taken and soaked in the hydrogen peroxide (H_2O_2) solution for 24 h to attain the carbonization activation. Then the samples were dried and washed with the distilled water and used for the final stage of the batch adsorption study.

2.2. Stock preparation

The Reactive Orange (16), Reactive Red (120) and Reactive Blue (19), commonly called azo dyes, were bought from Precision Scientific Chemicals, Coimbatore. These are analytical-grade dyes for which no cleansing is required. The dyes mentioned above are widely used in all kinds of textile industries creating toxic effects on the environment. In this experimental work, the stock solution was prepared by adding the three dyes individually in 1,000 ppm of double distilled water.

2.3. Batch adsorption studies

The adsorption of dyes using activated *P. juliflora* roots was investigated using the batch adsorption mode by varying pH levels, adsorbent dosage, concentrations, time of contact with adsorbent, and temperature of the solutions. In this experimental work, the characteristics of the adsorption process were adjusted accordingly: pH of the azo dye solution: 2–7, contact time: 10–120 min, adsorbent dose: 0.5–2.5 g·L⁻¹, dye concentration: 25–150 mg·L⁻¹, and temperature, 15°C–60°C. The prepared adsorbent was poured into the prepared synthetic solutions with known

concentrations. The conical flask was kept in the rotary shaker for continuous shaking for 60 min to attain equilibrium. The quantity of dyes adsorbed by the adsorbent was calculated using Eq. (1):

$$q_t = \frac{(C_0 - C_t)V}{m} \, \text{mg/g} \tag{1}$$

where q_t is the amount of dye adsorbed by the *juliflora* root at a time '*t*' and C_t represents the concentration of the dye in the solution at any time '*t*'.

The final suspension was taken from the rotary shaken after 5 min of centrifugal time. The amount of dye adsorbed after the complete adsorption process was found using UV-Visible Spectrophotometer. To get the concurrent value, each analysis was repeated two times, and the average value was considered. The number of dyes removed by *P. juliflora* root may be found with the help of data calculated from the batch study. The mass balance system for this adsorption process can be expressed using Eq. (2):

$$\%\text{Removal} = \left[\frac{C_0 - C_e}{C_e} \right] \times 100 \tag{2}$$

where C_o represents the initial concentration of the dyes in solution (mg·L⁻¹), C_e represents the equilibrium concentration of the dyes in solution (mg·L⁻¹), V represents the total volume of the solution, and m represents the mass of the adsorbent.

2.4. Scanning electron microscopy/energy-dispersive X-ray spectroscopy studies

The physical and elemental properties of activated juliflora roots during adsorption were evaluated by scanning electron microscopy-energy-dispersive X-ray spectroscopy (SEM-EDX) spectroscopy (JSM-6490V). The flaws and fractions, pollutants, and other particles existing on the adsorbent surface were identified using SEM analysis with a working distance of 10 μm, and voltage level at 20 kV. Two different SEM images analyzed the activated juliflora root's surface before and after receiving the azo dyes. To confirm the presence of selective azo dye on the surface of the adsorbent, EDX instrumental analyses were performed equipped with SEM.

2.5. Fourier-transform infrared spectroscopy analysis

The contribution of functional groups (carbonyl, hydroxyl, etc.) and their characterization was obtained using the Fourier-transform infrared spectroscopy (FTIR) techniques. It was also used to analyze the azo dyes and their chemical characteristics using the adsorbent material [22]. 0.5 g of juliflora root activated carbon powder was taken in the conical flask and mixed with 50 mg·L⁻¹ of azo dye concentrated synthetic solution having a pH of 2.0. The final supernatant was taken for FTIR analysis after 4 h of agitation of the prepared solution, its speed at 200 rpm. For scanning, the range was fixed from 4,000 to 400 with 4 cm⁻¹ resolution, and 20 scans were taken to obtain the spectra. The FTIR process was done before and after dye uptake by juliflora root adsorbent to compare the functional groups involved in the azo dye adsorption. The characterization of functional groups was used to identify the binding ability of the adsorbent, which is essential for all experimental processes [23].

2.6. Brunauer–Emmett–Teller surface area analysis

The surface area of activated *P. juliflora* roots was evaluated using the process of nitrogen adsorption at –196°C temperature. The activated adsorbent was allowed to heat at 300°C for 5 h to remove the gas molecules, and Brunauer calculated the vacuum and the area of the surface–Emmett–Teller (BET) was analysed.

2.7. Thermogravimetric analysis, derivative thermogravimetry and differential thermal analysis

The thermogravimetric and derivative thermogravimetric analyses were used to find out the mass and energy changes of the adsorbent at a high temperature. The thermogravimetric analysis (TGA) analysis will evaluate the number of materials removed from the adsorbent with increased temperature [24]. The derivative thermogravimetry (DTG) analysis will evaluate the removal rate of materials within the estimated time to find out the exothermic or endothermic adsorption process [25]. For the TGA and DTG analysis, 20 mg of *P. juliflora* root charcoal was taken and placed in the instrument to obtain the characteristics.

2.8. X-ray diffraction analysis

X-ray diffraction analysis was used to analyze the crystalline structure of the adsorbent material at the different peaks. The phases and sizes of crystalline structure were identified by operating the instrument with CuKα radiation and the power of 40 kV working at 250 mA. The characteristics of peaks were obtained from the analysis and compared in agreement with JCPDS standards using the reference code of 00-002-1035 [26].

2.9. X-ray photoelectron spectroscopy analysis

The X-ray photoelectron spectroscopy (XPS) analysis for the adsorbent material before and after taking azo dyes were performed using a thermos K-Alpha and XPS fitted with monochromated Al-kα X-ray source. With the high resolution of 40 eV scans the data were gathered by passing the energy of 2,150 eV. At a temperature of 20°C, the spectra were obtained under the pressure of 10⁻⁷ Torr. The obtained data was analyzed using CasaXPS and fitted with a Shirley background.

2.10. Isotherm studies

The adsorbent characteristics (size of the pore, volume, energy, etc.,) were assessed using the adsorption isotherm process. The curve plotted from the isothermal studies relates to the connection between azo dyes and *P. juliflora* root adsorbents and provides information of the specific desorption process [27]. To maximize the usage of *P. juliflora* root adsorbent, the isotherm studies were used to increase the connection between azo dyes and prepared adsorbent [28]. The adsorption mechanism was optimized based on the proper conclusions drawn from the equilibrium plots. The isotherm studies provide valuable data for a massive production system to examine the outputs [20]. It also supports the isotherm studies during the initial stages to obtain the optimum purity level of *P. juliflora* roots. This is especially crucial when the contaminants are present in one or more toxins [29]. The uptake level of materials (q_e) during the equilibrium time has been enabled in these isotherm studies. This can be used to obtain the various forms of adsorbents as an output.

2.10.1. Langmuir isotherm studies

The adsorption of toxic contaminants by the specific adsorbent was analyzed by the standard isotherm model called the Langmuir isotherm study. This model assumes that the binding action between the adsorbent and adsorbate happens mostly through chemical process [30]. The monolayer adsorption process was followed and preference was given to all active sites of the adsorbate material [31]. Also, the entire process of adsorption was of a homogeneous nature. The one active site reacts with the adsorbate without interaction, and the surface phase is a monolayer [32]. The expression for the Langmuir isotherm study is given by Eq. (3):

$$\frac{C_e}{q_e} = \frac{1}{Kq_{max}} + \frac{C_e}{q_{max}} \tag{3}$$

where C_e represents the equilibrium concentration of the dyes in solution (mg·L^{-1}), q_e – amount of adsorbate adsorbed per amount of adsorbent at equilibrium (mg·g^{-1}), q_{max} – maximum monolayer adsorption capacity (mg·g^{-1}), and K – constants of Langmuir isotherm equation related to capacity and intensity of adsorption.

2.10.2. Freundlich isotherm studies

Freundlich isotherm study allows multiple layers of adsorption on the surface of adsorbent [33]. The expression for the Freundlich isotherm study is given by Eq. (4):

$$\ln q_e = \ln k_f + \frac{1}{n}\ln C_e \qquad (4)$$

where q_e – adsorbed quantity of adsorbate per g, n – adsorption energy, k_f – capacity of adsorption related to Freundlich constant, and C_e – represents the equilibrium concentration of the dyes in solution (mg·L^{-1}).

2.10.3. Redlich–Peterson isotherm

The elements were incorporated from both Langmuir and Freundlich isotherm models, and the Redlich–Peterson isotherm was derived in a three-parameter empirical model. The basic assumption of this model is that the mechanism of adsorption is unique, and it does not follow the characteristics of monolayer adsorption [34]. The expression for this isotherm model is given in Eq. (5):

$$\ln\left(K_R\frac{C_e}{q_e}-1\right) = b_R\ln C_e + \ln a_R \qquad (5)$$

where K_R – adsorption capacity constant of Redlich–Peterson (R-P) isotherm obtained from the linear plots, a_R – R-P isotherm constant, and b_R – exponent value (0–1).

2.10.4. Sips isotherm

The Sips isotherm was derived from the Langmuir and Freundlich isotherm and their limiting behaviour levels. For the prediction of adsorption in the heterogeneous sites, this model is very suitable, and the limitations increased by the concentration of adsorbate are completely avoided [35]. Therefore, when the adsorbate concentration is very high, the Sips model forecasts the monolayer adsorption, that is, the Langmuir model. The linear equation for the Sips model is given by Eq. (6):

$$\frac{1}{q_e} = \frac{1}{Q_{max}K_S}\left(\frac{1}{C_e}\right)^{\frac{1}{n}} + \frac{1}{Q_{max}} \qquad (6)$$

where Q_{max} and K_S – adsorption capacity and equilibrium constant obtained from the slope and intercept in linear plots and n – factor of heterogeneity lies between 0 to 1.

2.10.5. Toth isotherm

To reduce the discrepancies between the experimental data obtained and the equilibrium predicted value of the Langmuir isotherm, the Toth isotherm was derived with some modifications. Even at low and very high concentrations, this model will describe the adsorption system [36]. The linear equation for the model is given by Eq. (7):

$$\ln\frac{q_e}{q_m - q_e} = n\ln K_L + n\ln C_e \qquad (7)$$

where K_L and n is called Toth isotherm constant in mg·g^{-1} and q_e – quantity of materials adsorbed in equilibrium mg·L^{-1}.

2.10.6. Fritz–Schlunder isotherm

The coefficients of the isotherms fall within a wide range, and the experimental data is very high; the four-parameter isotherm model (Fritz–Schlunder) was used, which is derived from the empirical equation [37]. The linear model isotherm equation is given by Eq. (8):

$$q_e = \frac{q_{mFS}K_{FS}C_e}{1 + q_m C_e^{MFS}} \qquad (8)$$

where q_{mFS} is called maximum adsorption capacity in mg·g^{-1}, K_{FS} – equilibrium constant in mg·g^{-1}, and MFS – model exponent.

2.11. Kinetic studies

Equilibrium time is critical for aqueous solutions in the batch adsorption process. It provided the needed data related to the efficiency of adsorption and the possibility of scale-up procedures. The following kinetic studies were performed in this entire research work.

2.11.1. Pseudo-first-order

Pseudo-first-order (or) Lagergren model was established for the liquid and solid systems adsorption from the aqueous medium depending upon the capacity of solid adsorption [38]. This model was based on the basic assumption that the driving force is directly proportional to the rate of adsorption [39]. The difference between initial concentration (q_e) and equilibrium concentration (q) can be used to evaluate the process of adsorption.

The pseudo-first-order model is expressed as given by Eq. (9):

$$\frac{dq_e}{dq_t} = k(q_e - q_t) \qquad (9)$$

At the equilibrium, the total volume of azo dyes' uptake by the adsorbent at a time (t) was obtained by calculating q_e and q_t. Using the boundary layer conditions, Eq. (9) can be rearranged as Eq. (10):

$$\log(q_e - q) = \log q_e \frac{k}{2.303}t \qquad (10)$$

2.11.2. Pseudo-second-order

The second-order chemical adsorption process was used in this model, and it assumes that the number of squares of empty sites is directly proportional to the adsorption rate [40].

The pseudo-second-order model is expressed by Eq. (11):

$$\frac{d_q}{d_t} = k\left(q_e - q\right)^2 \tag{11}$$

By applying boundary conditions ($t = 0$ to $t > 0$, and $q = 0$ to $q > 0$), the Eq. (6) can be rearranged as Eq. (12):

$$\frac{t}{q} = \frac{1}{h} + \frac{1}{q_e}t \tag{12}$$

where $h = kq_e^2$ – initial adsorption rate and k – rate constant. The plot of t/q_t vs. time at various adsorption limits provides a linear relationship, allowing the determination of q_e, k and h.

3. Results and discussion

3.1. SEM analysis

Fig. 3a shows the SEM images of raw *P. juliflora* roots before the adsorption of dyes from synthetic solutions. The uneven pores on the surface of the adsorbent were used to receive the pollutants from the aqueous solutions. Fig. 3b shows the SEM images of charcoal-based adsorbent activated by hydrogen peroxide. The figure shows that the activated charcoal adsorbent has a very high surface area and volume compared to the raw adsorbent. The uneven pores were identified on the surface of the activated adsorbent and was found to be in higher range than the raw adsorbent [41]. Due to the hydrogen peroxide activation process, the adsorbent reacted with the activating agent and produced uneven pores [42]. These are very helpful in receiving/attracting the various pollutants from the aqueous solutions. Compared to the raw adsorbent material, activated carbon charcoal-based adsorbent adsorbs a more significant number of pollutants from the aqueous medium [43]. From the figure, the cloud formation on the top side of the adsorbent material can be seen. Also, there are no vacant sites available on the surface of the adsorbent, which confirms that adsorption has taken place. Also, the synthetic dyes react with the charged sites and protonate, which has not destroyed the functional group existing in the adsorbent [44]. The targeted azo dyes Reactive Orange – RO-16, Reactive Red – RR-120 and Reactive Blue – RB-19 and their presence in the adsorption process was confirmed by the following EDX analysis.

3.2. EDX analysis

Energy-dispersive X-ray analysis was used to identify the components adsorbed by the prepared adsorbent. In this
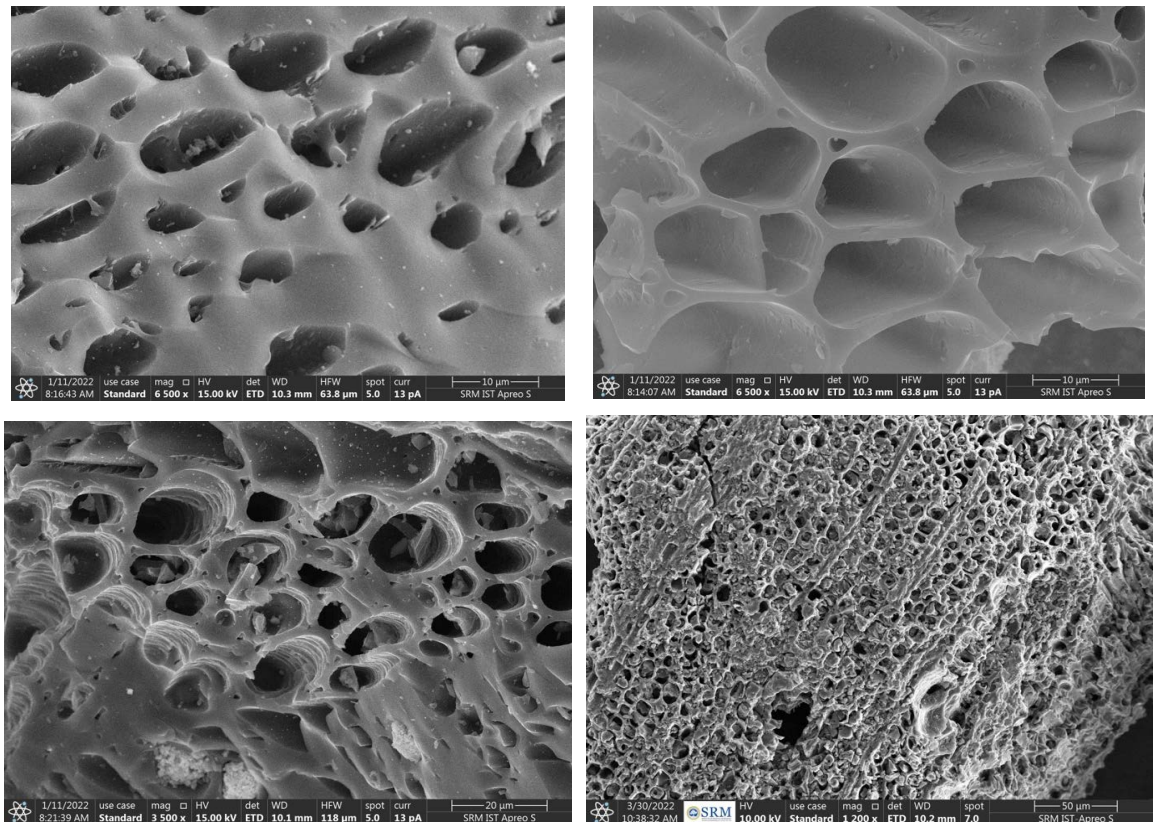

Fig. 3. SEM images of: (a) raw adsorbent before adsorption and (b) charcoal adsorbent after the adsorption of azo dyes.

experimental work, the EDX analysis was performed individually to confirm the adsorption of azo dyes. Fig. 4a shows the EDX image of raw *P. juliflora* root powder and 4b shows the charcoal juliflora activated adsorbent after the adsorption of pollutants from the aqueous solutions. Referring to Fig. 4a, the presence of carbon, oxygen, and calcium elements was observed. However, Fig. 4b shows the organic and inorganic functional groups after converting the raw adsorbent into charcoal by chemical and physical synthesis. Further, the prepared charcoal adsorbent was activated using the hydrogen peroxide solution. The synthetic solution was passed into the activated adsorbent to adsorb the azo dyes and other toxic contaminants [45]. Fig. 4b shows the EDX image of adsorbent material after the passage of dye solution. Many organic and inorganic pollutants and their adsorption were observed in that picture, and it confirms the adsorption of the targeted dyes by activated juliflora adsorbent.

3.3. FTIR analysis

The FTIR spectrum of *P. juliflora* root powder is shown in Fig. 5a and b taken at two different stages (before and after adsorption of the pollutants). In these figures the high energy region was noticed in the band level of 3,420 and 2,860 cm^{-1}, confirming –OH and –CH$_2$ groups [46]. The level between 1,000–1,800 cm^{-1}, various functional groups may be categorized, that is, band 1,620 cm^{-1} shows the presence of water; band 1,460–1,600 cm^{-1} shows the aromatic vibrations, band 1,380–1,400 cm^{-1} shows the presence of bending vibrations by the –CH$_2$ functional group, and band 1,080 cm^{-1} shows the vibrations by C–O functional groups [6]. The band goes below 1,000 cm^{-1}, and C–H bending exists due to the aromatic vibrations. The lower frequencies indicate the –OH stretching due to the aromatic ring vibrations, and the stretching vibrations by –CH$_2$ disappeared at 2,860 cm^{-1}. Based on the FTIR studies, the presence of functional groups
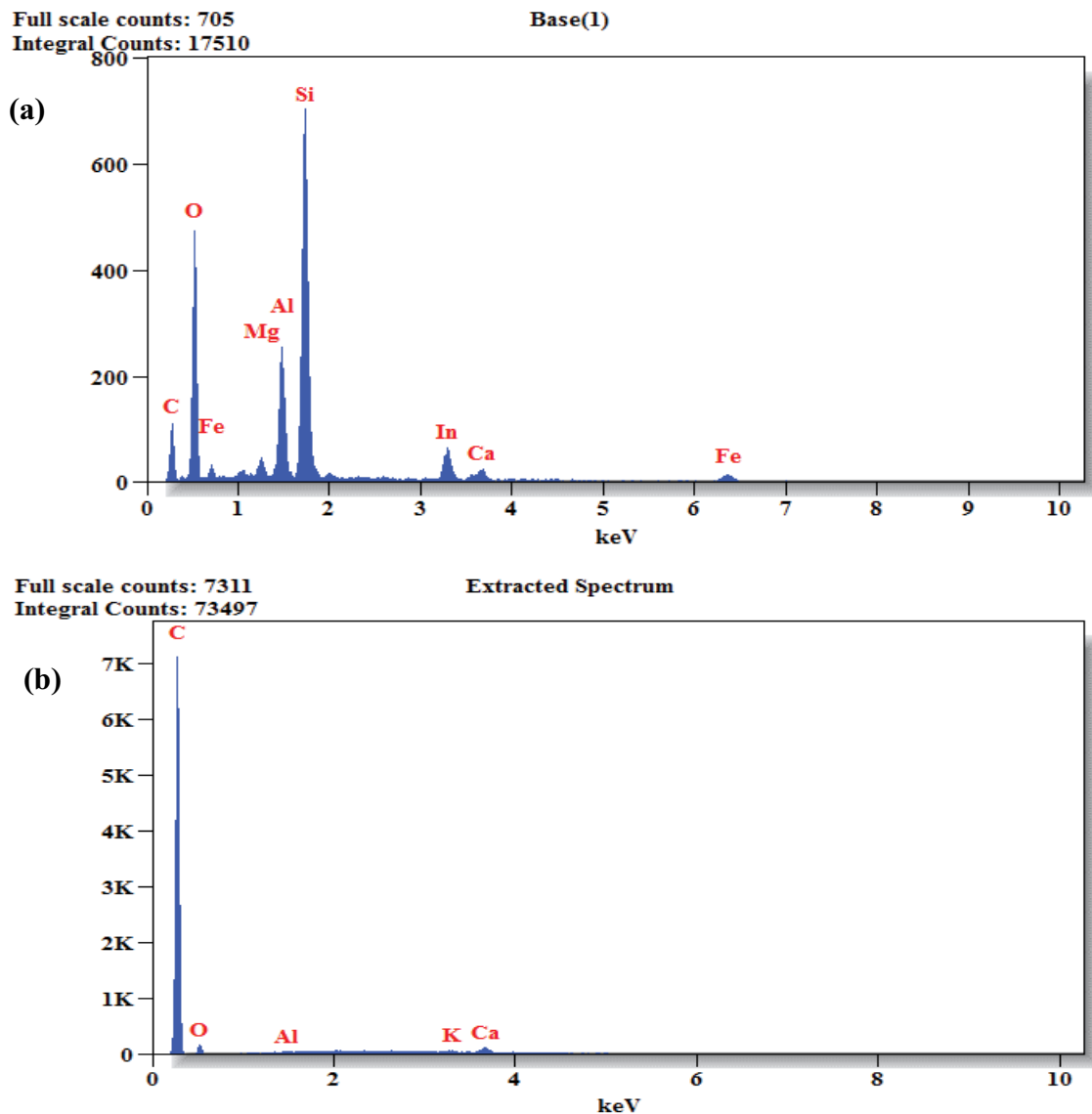

Fig. 4. EDX images of: (a) raw adsorbent and (b) activated charcoal adsorbent after the adsorption of azo dyes.
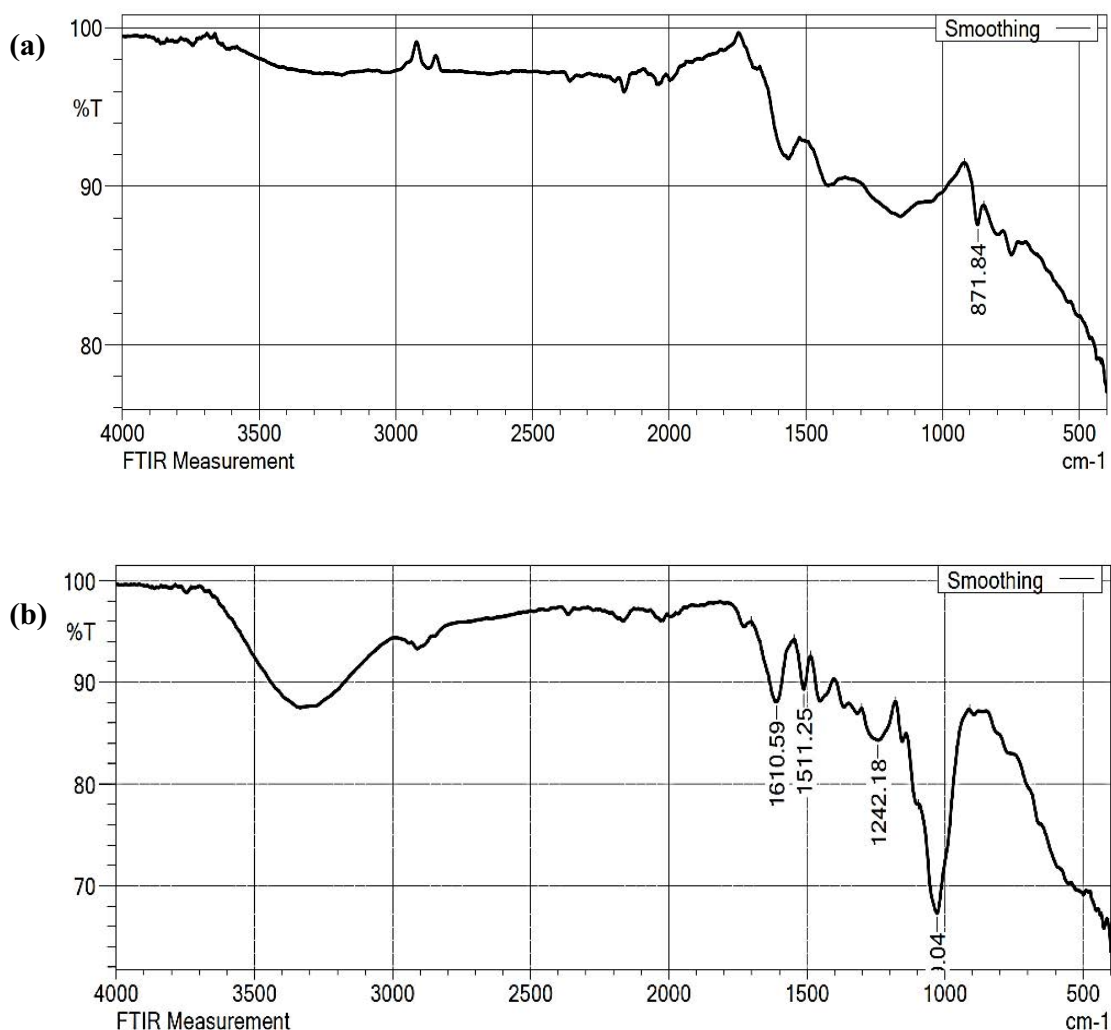
Fig. 5. FTIR spectra of: (a) raw adsorbent and (b) azo dyes adsorbed adsorbent.

confirms the ability of prepared *P. juliflora* adsorbent to receive the pollutants from the aqueous solutions during the adsorption process.

3.4. TGA, DTG and differential thermal analysis

The analysis of TG and DT of prepared *P. juliflora* charcoal adsorbent is represented in Fig. 6a and b for raw and charcoal-based *P. juliflora* root adsorbent under various temperatures. The presence of organic functional groups was observed on the surface of the adsorbent. By varying the heat up to 900°C at 10°C·min⁻¹ rates of heating, the *P. juliflora* root charcoal was exposed for the analysis. Three stages of adsorbent decomposition were identified from the plot, representing the material's heat absorbance. The loss in weight was observed up to 600°C due to dehydration of the adsorbent material, and beyond that temperature, a constant rate was attained [32]. The maximum peak observed at the temperature of 400°C may represent the endothermic nature of *P. juliflora* root charcoal [47]. The presence of functional groups in the charcoal adsorbent was identified when the

process reached the saturation level at 900°C. Based on the above observations, the prepared *P. juliflora* root-activated carbon has very high stability in temperature.

3.5. BET surface area analysis

The process of adsorption and desorption in BET surface area analysis is shown in Fig. 7, and its characteristics are good in contact with the process. Referring to Fig. 7, the curves show the isotherm follow up under type II, representing that *P. juliflora* root activated charcoal contains both micro and mesopores [48]. Due to the multilayer adsorption process, the first part in the isotherm part represents the micropores, and the second part represents the mesopores by relative pressure [49]. The *P. juliflora* activated charcoal root has a surface area of 57.747 m²·g⁻¹, smaller than average carbons, with a pore volume of about 0.094 cm³·g⁻¹ and pore radius of 14.881 Å. The characteristics of raw and charcoal *P. juliflora* adsorbent is given in the Table 1 and compared to raw adsorbent. The activated charcoal *P. juliflora* adsorbent has very high surface area and pore volume.
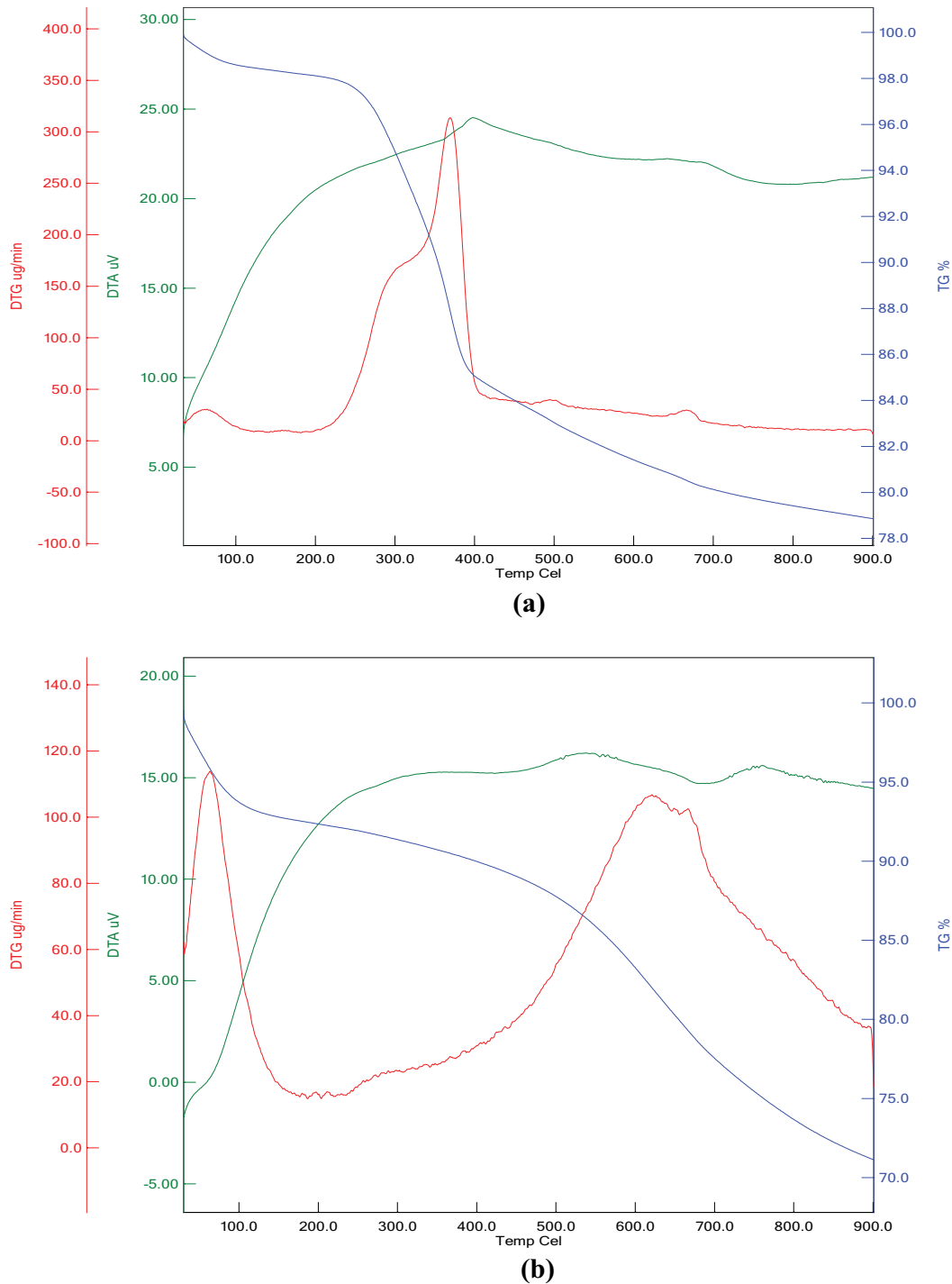
(a)

(b)

Fig. 6. TGA, DTG and DTA plots for (a) raw adsorbent and (b) activated charcoal-based adsorbent.

3.6. X-ray diffraction analysis

The X-ray diffraction (XRD) peaks of raw adsorbent and activated prosopis charcoal adsorbent is shown in Fig. 8a and b, respectively. Compared to the raw adsorbent, the charcoal adsorbent has very high intensity and amorphous structure. The activated *P. juliflora* root charcoal are in good agreement with the peaks of 160, 240, 280, 311, 395 and 480 at 2θ matches with 80, 110, 60, 40, 35 and 20 hkl

planes, respectively. Based on the diffraction points and their high pitching, the amorphous nature and intensity of the adsorbent material was confirmed [50].

3.7. XPS analysis

The XPS analysis of adsorbent material is shown in Fig. 9 under three stages. The natural adsorbent generated the peaks at 300 and 550 eV indicating the presence of various
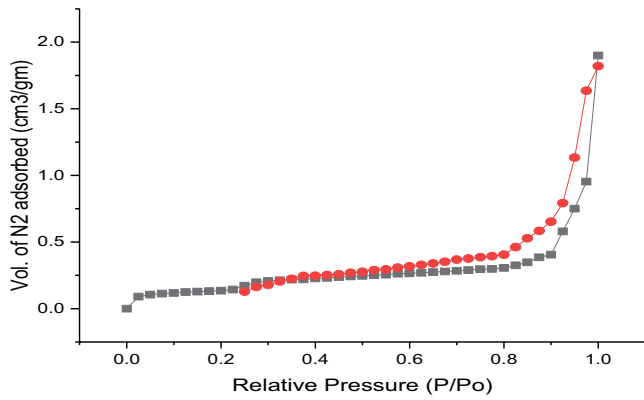
Fig. 7. Adsorption–desorption isotherm study of *Prosopis juliflora* root charcoal adsorbent.

Table 1
Pore characteristics of raw and activated charcoal *Prosopis juliflora* adsorbent

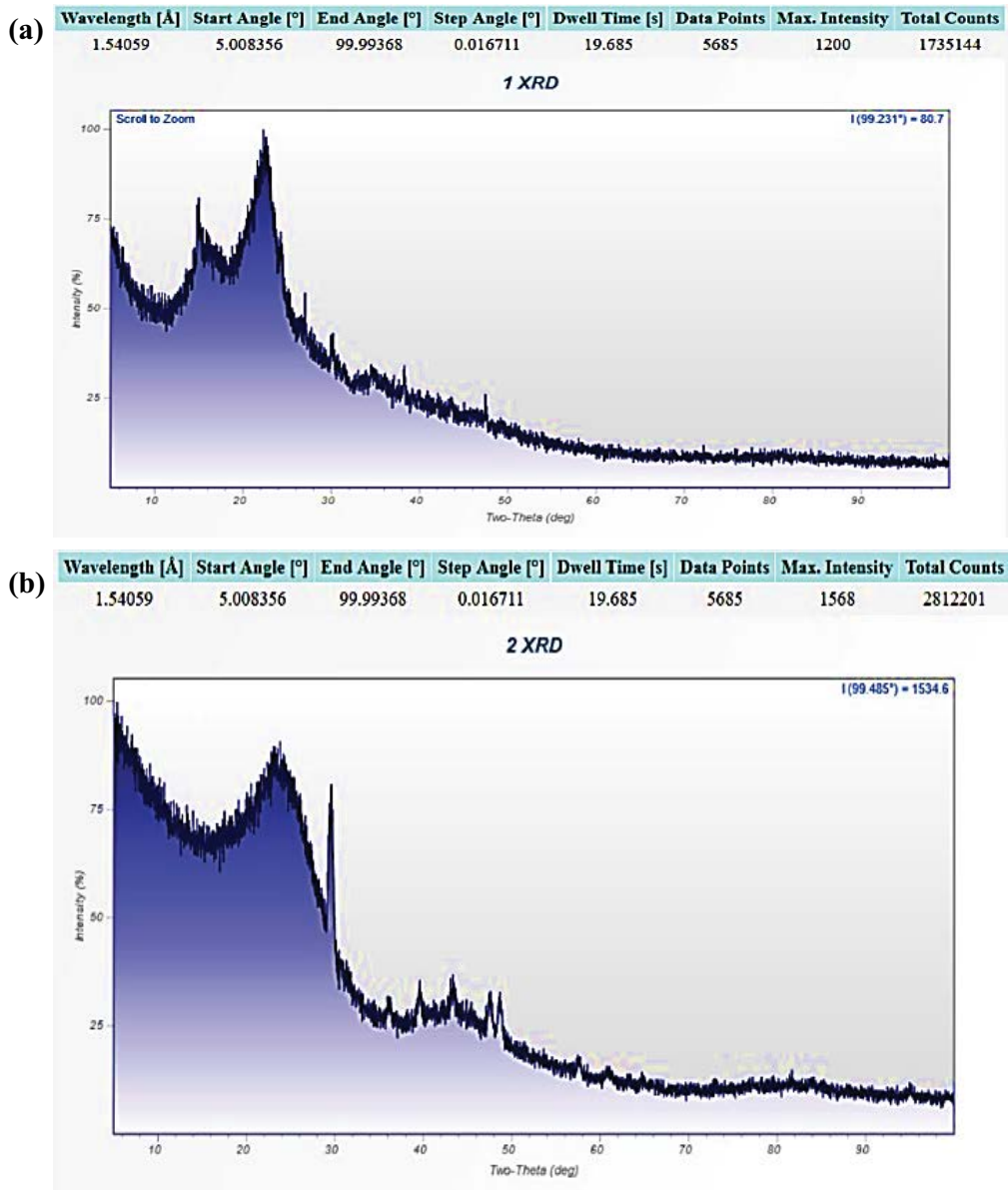| Parameter	Raw adsorbent	Activated charcoal adsorbent
BET surface area, $m^2 \cdot g^{-1}$	41.352	57.747
Pore volume, $cm^3 \cdot g^{-1}$	0.072	0.094
Micropore volume, $cm^3 \cdot g^{-1}$	0.128	0.189
Mesopore volume, $cm^3 \cdot g^{-1}$	0.096	0.082
Micropore area, $m^2 \cdot g^{-1}$	413	392
Average pore radius, Å	17.284	14.881

Fig. 8. XRD analysis of: (a) raw and (b) *Prosopis juliflora* roots activated charcoal.

Fig. 9. XPS spectra of adsorbent material.

Fig. 10. Adsorption of RO-16, RR-120 and RB-19 dyes by varying the pH using *Prosopis juliflora* roots activated charcoal.

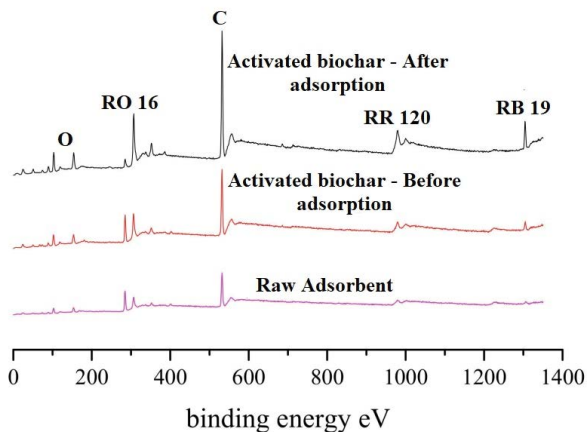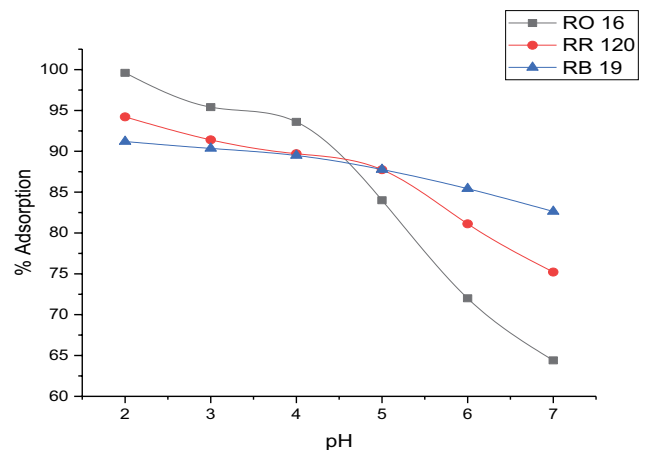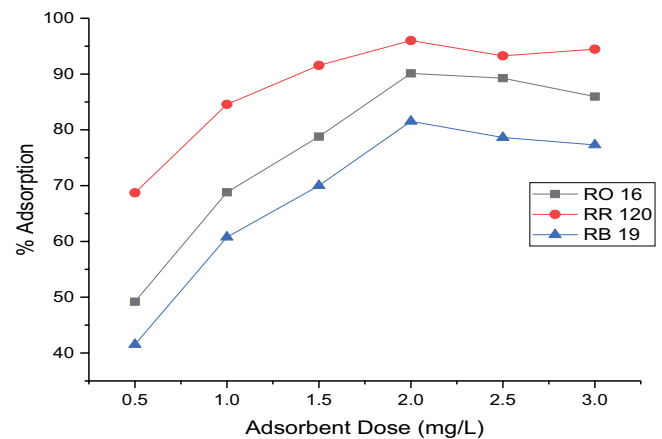Fig. 11. Adsorption of RO-16, RR-120 and RB-19 dyes by varying the dose level using *Prosopis juliflora* roots activated charcoal.

functional groups. Then the activated biochar adsorbent before taking the azo dyes was shown in the second line. It indicates the various functional elements at the band energy of 550 eV due to the high amount of carbon. After the azo dye uptake by the adsorbent material, many peaks were observed. The targeted azo dyes of RO-16 at 320 eV, RR-120 at 980 eV and RB-19 1,300 eV band levels were observed. Also, a huge amount of carbon and its presence were obtained at the peak of 550 eV. Based on the XPS studies and the peak values, the adsorbent material has a very good ability to receive the pollutants from the aqueous medium.

3.8. Influence of pH in dye removal

The power of hydrogen (pH) of the synthetic solution has been adjusted from 2 to 7, and its influence on the adsorption of azo dyes was examined in this batch adsorption study. When the azo dye-containing solution's pH was increased gradually, it was seen that a stable decrease in the percentage of dye adsorption in Fig. 10. The presence of positively charged adsorbents on the surface reduces the interface between azo dyes and the *P. juliflora* roots [51]. The adsorbent surface developed in a low positive charge during the pH of the solution is very low and simulated the faster removal of azo dyes [46]. The maximum amount of dye removal was obtained at the pH of 2.0, and a gradual decrement in the amount of adsorption was noticed when the pH of the solution was increased. Due to the hydroxide's precipitation and its attribution, a decrease in dye removal was noticed at higher pH levels [52]. The *P. juliflora* root activated carbon adsorbs 99.6% of Reactive Orange 16, 94.43% of Reactive Red 120, and 82.26% of Reactive Blue -19 dyes at the optimum pH of 2.

3.9. Influence of adsorbent dose in dye removal

The adsorbent dose level plays a vital role in removing pollutants from the aqueous medium. The dose level for the dye removal was adjusted from 0.5 to 2.5 g·L^{-1} with 0.5 g·L^{-1} of intervals, and the impact of dye adsorption was analyzed (Fig. 11). While increasing the adsorbent dose level, the availability of active sites gets increases, and the efficiency of azo dye removal also increases due to increases in active sites [29]. The maximum amount of dye removal, that is, RO – 93.45%, RR – 78.7%, and RB – 60.2%, was obtained at the optimum adsorbent dose level of 2 g·L^{-1} and a gradual decrement of the amount of adsorbent was noticed when the amount of adsorbent level goes above 2 g·L^{-1} due to the decrease in concentration gradient. This is because of free surface availability at the time of dye removal by the adsorbent [53].

3.10. Influence of contact time in dye adsorption

The influence of the concentration of the azo dyes was investigated by varying the contact time between the adsorbent and azo dyes from 10 to 120 min and adjusting the concentration of dyes from 25 to 150 mg·L^{-1}. The azo dye uptake by the adsorbent is rapid during the earlier stages because of the availability of the vacant sites in the adsorbent. Also, the dyes get saturated levels in the mesopores of the adsorbent [54]. Referring to Fig. 12, it was noticed
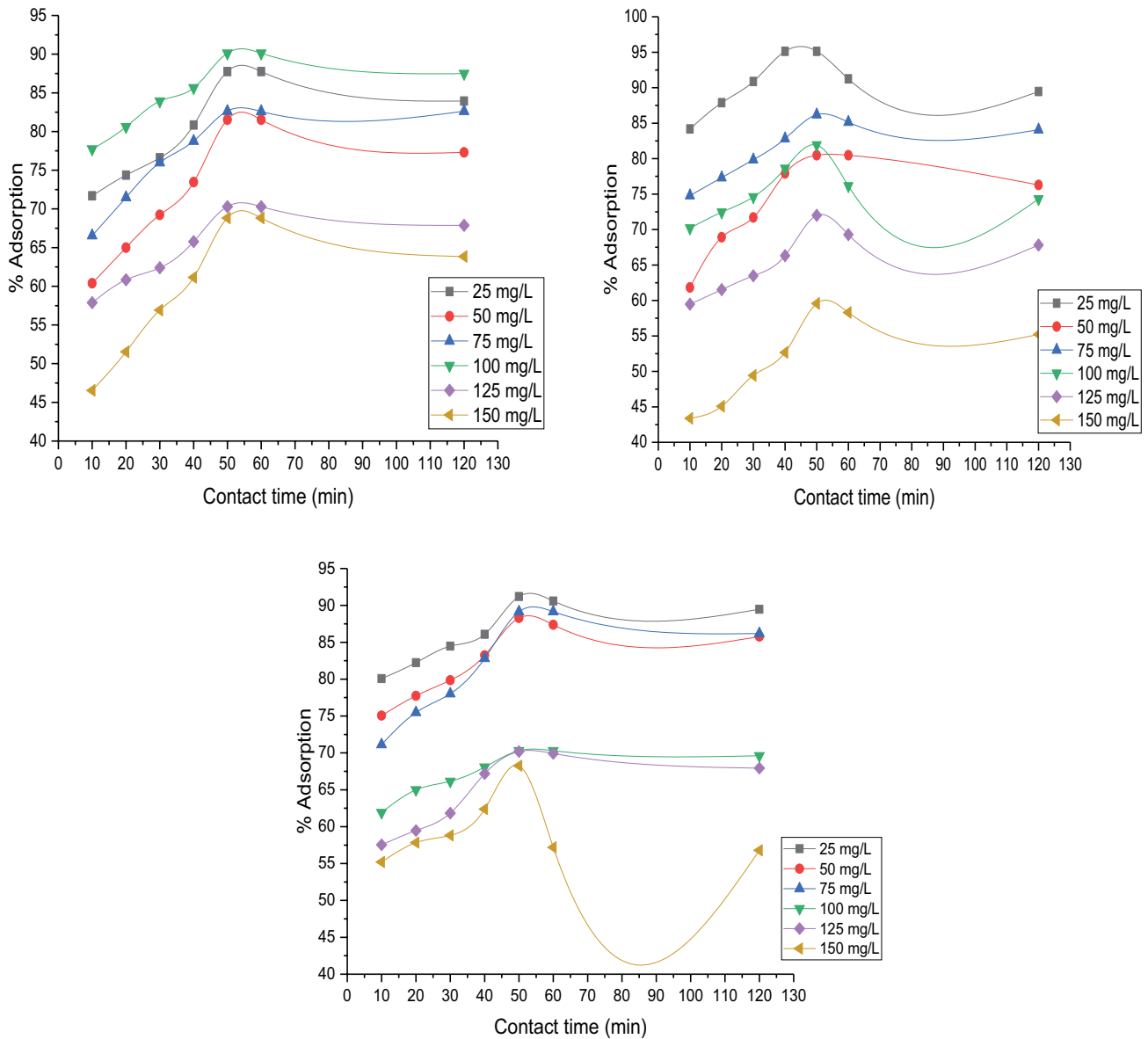
Fig. 12. Adsorption of RO-16 (a), RR-120 (b) and RB-19 (c) dyes by varying the contact time using *Prosopis juliflora* roots activated charcoal.

that after 50 min, there is no change in the amount of dye adsorption, and it attains the constant rate due to the repulsive force on the adsorbent molecule surfaces, that is, the mass transfer between the solid and liquid phases decreases with time [55]. Also, the azo dyes need a higher strength to travel into the pores on the adsorbent, which reduces the amount of adsorption in the final stages.

3.11. Influence of temperature in dye adsorption

The azo dye concentration was taken as 25 mg·L^{-1} with 2 g·L^{-1} of *P. juliflora* adsorbent; the temperature influence was investigated under various conditions (15°C–45°C) in the batch adsorption study for 50 min. Referring to Fig. 13, initially, the amount of azo dye uptake was rapid up to a temperature of 30°C, and sudden decrement was observed

beyond that optimum temperature. The drop in percentage adsorption at 30°C might be attributed to the desorption rate [54].

3.12. Influence of azo dye concentration in adsorption

The concentration of azo dyes in the solution was adjusted from 25 to 150 mg·L^{-1} in this batch study by fixing the concentration of *P. juliflora* powder adsorbent as 2 g·L^{-1} and other parameters fixed as constant. When the concentration of azo dyes is deficient, the availability of vacant sites is high, and rapid adsorption takes place at that particular time [56]. Furthermore, the concentration of azo dyes was gradually increased, and a sharp decrease in the amount of adsorption is identified in Fig. 14. The azo dyes adsorbed by the adsorbent get saturated in the mesopores
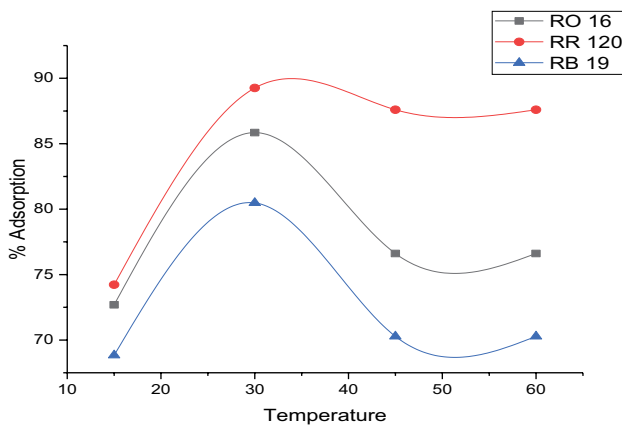
Fig. 13. Adsorption of RO-16, RR-120 and RB-19 dyes by varying the temperature using *Prosopis juliflora* roots activated charcoal.
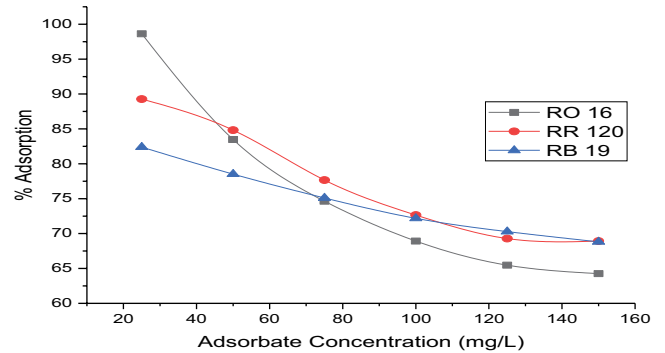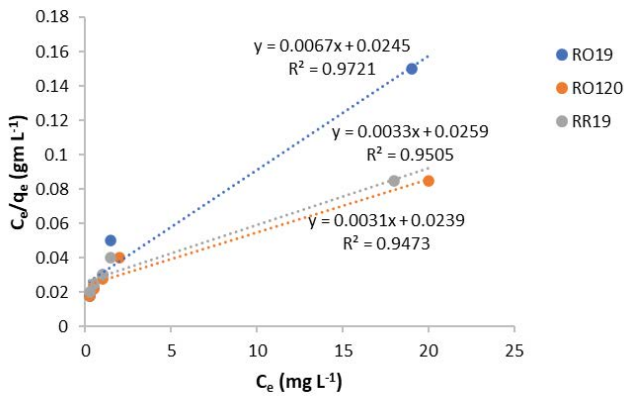

Fig. 14. Adsorption of RO-16, RR-120 and RB-19 dyes by varying the concentration of azo dyes using *Prosopis juliflora* roots activated charcoal.

[57]. The *P. juliflora* activated charcoal powder adsorbed 98.36% of RO-16, 89.72% of RR-120, and 82.93% of RB-19 azo dyes in low primary concentrations. The amount of azo dye uptake by the *P. juliflora* root powder was rapid in lower concentrations, indicating the adsorbent has not stretched the overload level [58].

3.13. Isotherm studies

3.13.1. Langmuir study

The isotherm plots (C_e/q_e vs. C_e) are shown in Fig. 15, which indicates the linearity, and the constants of the Langmuir isotherm model (k, q_{max}) were attained from the plots. The coefficient of regression was calculated at 30°C represented in Table 2. For 25 mg·L^{-1} of azo dye concentration, separation parameters were 0.0033 for RO-16, 0.0160 for RR-120, and 0.0295 for RB-19 azo dyes. The values are 0 to 1, which indicates the excellent adsorption process [59].

Fig. 15. Langmuir isotherm plots for azo dye uptake using *Prosopis juliflora* roots activated charcoal.

Table 2
Adsorption isotherm constants for azo dye adsorption using *Prosopis juliflora* root charcoal adsorbent

Model	Parameters	RO-16	RR-120	RB-19
Langmuir	q_{max}	9.402	9.929	10.434
	K_L	0.343	0.174	0.109
	R^2	0.9721	0.9505	0.9473
Freundlich	k_f	2.541	1.832	1.389
	n	2.963	2.315	2.026
	R^2	0.9546	0.9602	0.9912
Redlich–Peterson	K_{R-P}	11.325	6.28557	4.5350
	α_{R-P}	0.32684	0.13132	0.0744
	β_{R-P}	1.05217	1.14532	1.2139
	R^2	0.9571	0.9875	0.9868
Sips	K_S	12.8689	6.13959	3.7113
	β_S	1.25346	1.54742	1.6536
	a_S	0.47347	0.24345	0.1544
	R^2	0.9182	0.9599	0.9991
Toth	Q_{max}	27.4598	25.4221	24.0547
	b_T	0.38393	0.22272	0.1699
	n_T	0.78414	0.58286	0.4973
	R^2	0.8287	0.8224	0.829
Fritz–Schlunder	q_{mFS}	0.33127	0.00426	0.0744
	K_{FS}	34.3899	157.297	60.9892
	N_{FS}	1.05062	0.4444	1.2140
	R^2	0.9411	0.9614	0.9545

3.13.2. Freundlich isotherm study

Freundlich isotherm constants (k_f and n) was calculated from the linear plots (lnq_e vs. lnC_e) at 30°C (Fig. 16), and values are represented in Table 2. The calculated n values of 3.420 for RO-16, 2.779 for RR-120, and 2.384 for RB-19 dyes between 1 to 10 indicate the physical adsorption of azo dyes and the adsorbent. Both Langmuir and Freundlich isotherm were analyzed using the same set of experimental data. Based on the regression values (R^2) obtained from the plots, Langmuir and Freundlich isotherm model show strong evidence of the adsorption process [60].

3.13.3. Redlich–Peterson isotherm

The constants of this model (K_R and a_R) were obtained from the linear plot of this isotherm study by referring to Fig. 17, and the values are listed in Table 2. The R-P isotherm studies are more accurate than other isotherm studies because of three unknown parameters [61]. The b_R values lie between 0 to 1, representing the model's fitting, either Langmuir or Freundlich type. When the value of b_R is equal to 1, it becomes the Langmuir isotherm fit, and b_R equals 0, representing the Freundlich isotherm fitting method.

3.13.4. Sips isotherm

The constants of the Sips model Q_{max} and K_S were obtained by taking slope and deflection values from the kinetic linear plots of this model (Fig. 18). The values of constants and regression standards are represented in Table 2. The coefficient of regression (R^2) value is more than 0.95, which indicates the fitting process of dye adsorption. Based on the heterogeneity factor (n) value, the model describes the nature of fitting, and the value of n lies between 0 to 1. If the n value reaches 1, this equation reduces to the Langmuir equation, and it infers the adsorption process in homogeneous nature [62].
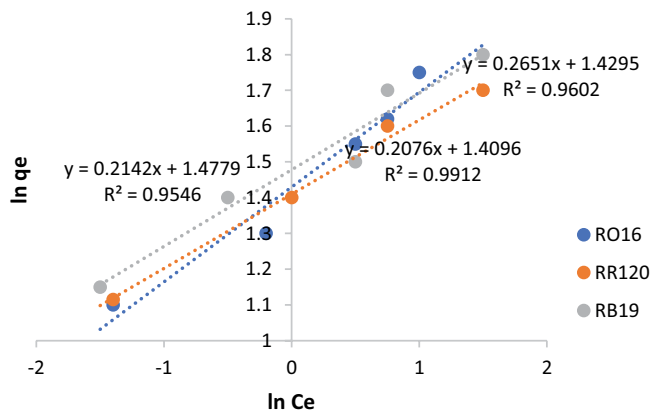
3.13.5. Toth isotherm

The linear plot for the Toth isotherm model is shown in Fig. 19, and its constants values were obtained from the slope and deflection values from the plots and listed in Table 2. To identify the heterogeneous solid surfaces, the Toth

Fig. 18. Sips isotherm plots for azo dye uptake using *Prosopis juliflora* roots activated charcoal.

Fig. 16. Freundlich isotherm plots for azo dye uptake using *Prosopis juliflora* roots activated charcoal.

Fig. 19. Toth isotherm plots for azo dye uptake using *Prosopis juliflora* roots activated charcoal.

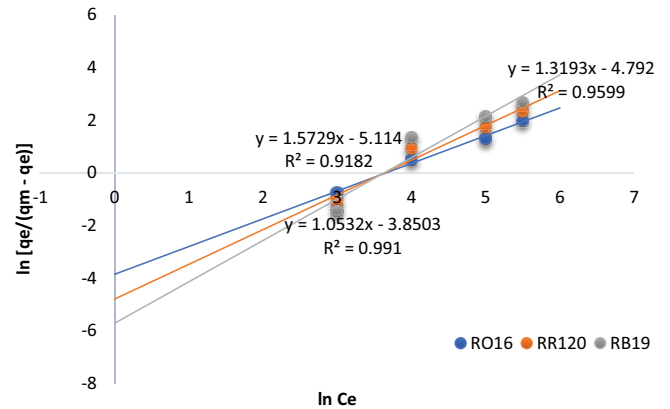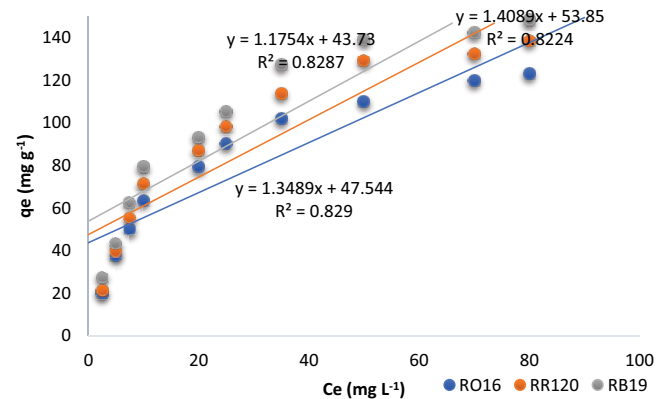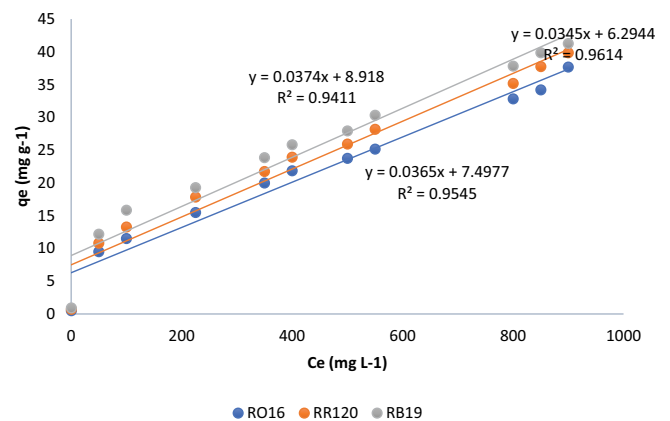Fig. 17. R-P isotherm plots for azo dye uptake using *Prosopis juliflora* roots activated charcoal.

Fig. 20. Fritz–Schlunder isotherm plots for azo dye uptake using *Prosopis juliflora* roots activated charcoal.
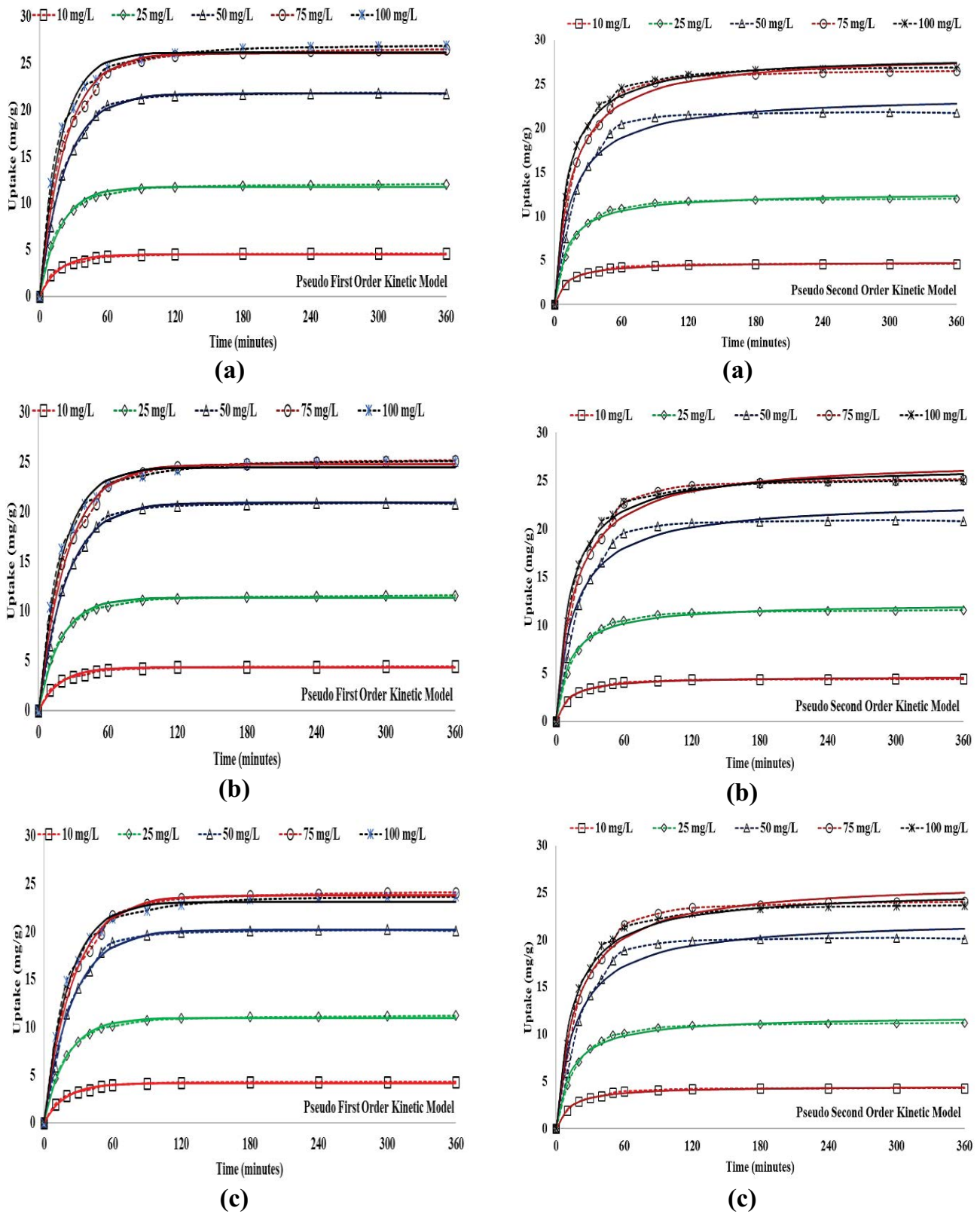
Fig. 21. Pseudo-first-order and pseudo-second-order kinetic plots for: (a) RO-16, (b) RR-120 and (c) RB-19 – azo dyes adsorption by *Prosopis juliflora* root charcoal.
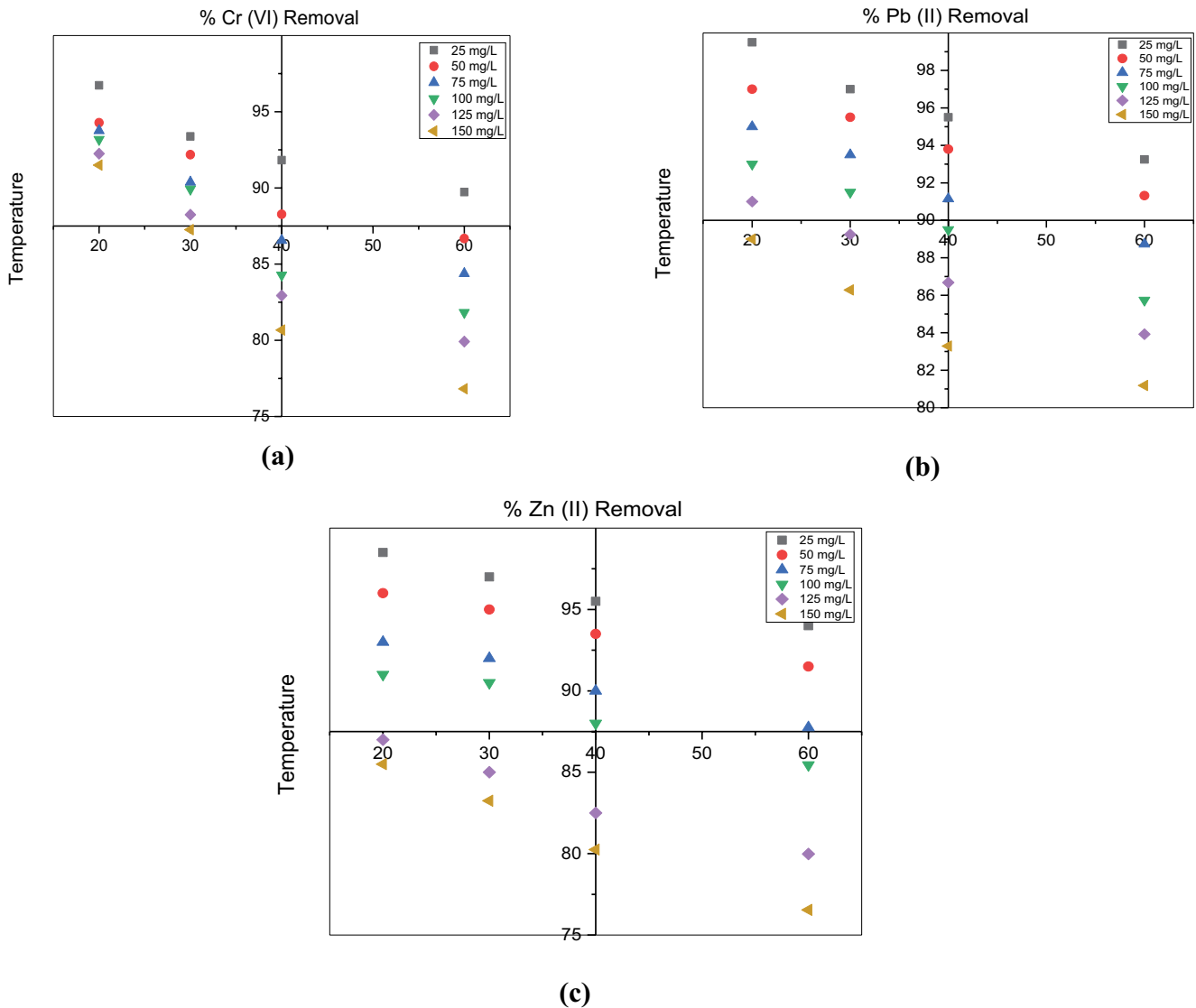
(a)

(b)

(c)

Fig. 22. Impact of temperature in: (a) RO-16, (b) RR-120 and (c) RB-19 dye adsorption using activated *Prosopis juliflora* roots activated charcoal.

isotherm study was used. This model, also called the three-parameter model, analyzed the interaction effects between the surfaces adsorbed with the azo dyes [63]. Referring to the linear isotherm plots, the regression coefficient values were shallow ($R^2 < 1$), which indicates the non-suitability of the adsorption process. The Toth isotherm plots were used to connect the equilibrium data if the Langmuir isotherm was not fitted properly with the adsorption process [64].

3.13.6. Fritz–Schlunder isotherm

This type of isotherm is usually called a four-parameter isotherm model to analyze the adsorption variation with pressure and temperature [65]. Fig. 20 shows the linear plots of this isotherm study, and the constants of the Fritz–Schlunder isotherm are represented in Table 2. The correlation coefficient (R^2) values were obtained from the linear plots, which are lower than the other isotherm studies, indicating the non-applicability of the adsorption process [23]. Based on the above discussions, the following isotherm models, Langmuir, Freundlich, R-P and Sips, were fitted well with the adsorption process, confirming the dye uptake by *P. juliflora* root charcoal indicates is homogeneous and monolayer adsorption. The other isotherm studies such as Toth, Fritz–Schlunder were more or less fitted very well with any one of the azo dye adsorptions by *P. juliflora* root charcoal adsorbent.

3.14. Kinetic studies

3.14.1. Pseudo-first-order kinetic study

This kinetic study may describe the kinetics of adsorption. The pseudo-first-order kinetic plots (($q_e - q$) and (t)) are shown in Fig. 21 for RO-16, RR-120 and RB-19 azo dyes, respectively. Adjusting the concentrations of dye solutions
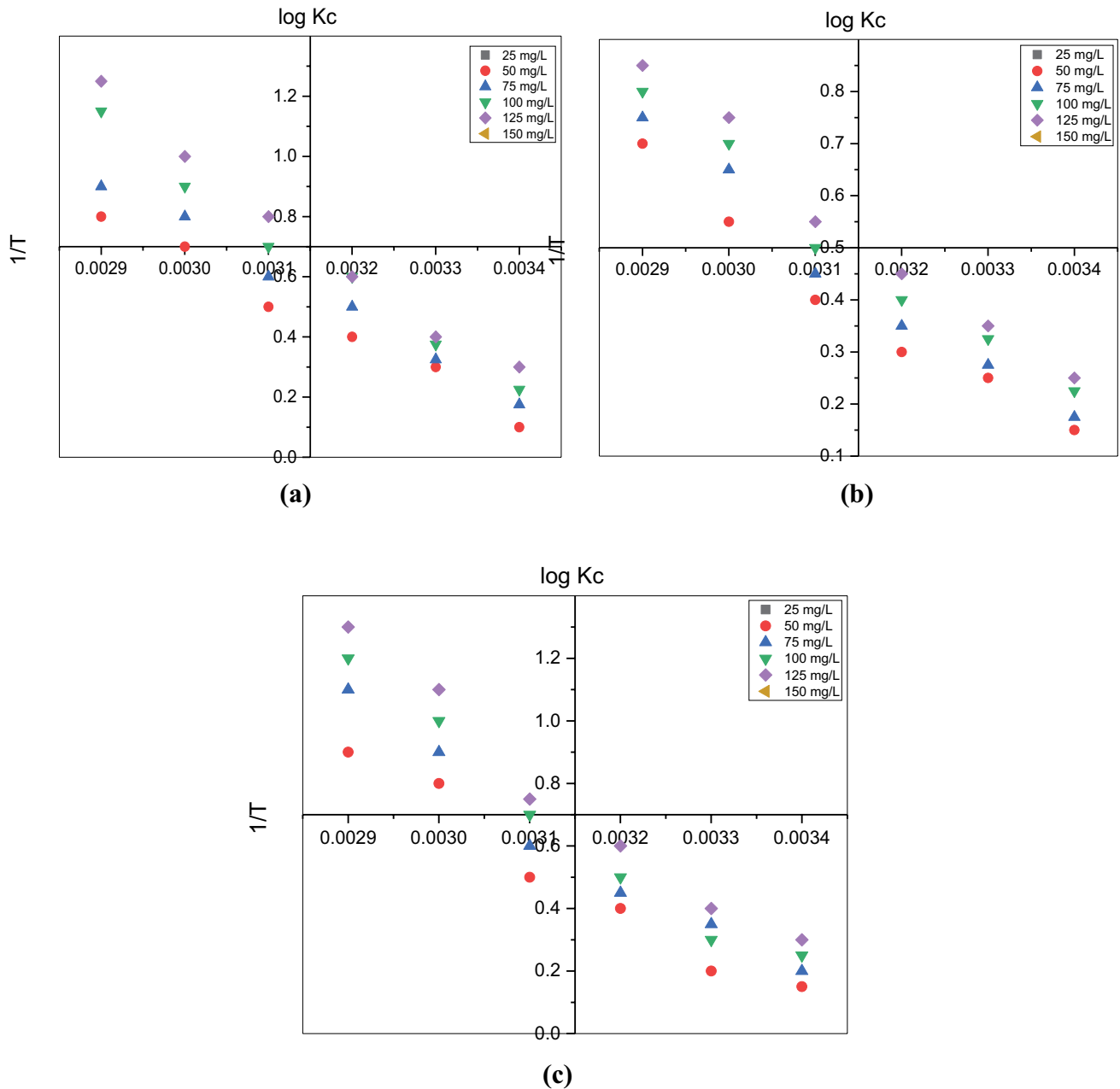
Fig. 23. Thermodynamic plots for: (a) RO-16, (b) RR-120 and (c) RB-19 dye adsorption using *Prosopis juliflora* roots activated charcoal.

from 25 to 150 mg·L⁻¹, the kinetic constant (k) and regression values (R^2) were obtained using the first-order kinetic plots and represented in Table 3. Referring to Table 3, the calculated R^2 values are low. It indicates the non-applicability of this kinetic study, which concludes that the process of adsorption has not attained the equilibrium level [66].

3.14.2. Pseudo-second-order kinetic study

The concentrations of the azo dyes in the synthetic solution have been adjusted from 25 to 150 mg·L⁻¹, and the pseudo-second-order plots (t/q vs. t) were plotted and shown in Fig. 21. The second-order kinetic constants were obtained based on the slope and intercept of linear plots and

represented in Table 4. The values obtained from the experimental (q_e) investigations are nearly similar to the calculated (q_e) values, and the regression values R^2 are more than 0.95, which indicates the applicability of this kinetic model and the process of adsorption has reached the conditions of equilibrium [67].

3.15. Thermodynamic studies of adsorption process

The temperature was adjusted from 15°C to 45°C, experimental investigations were done, and the impact of azo dye uptake by *P. juliflora* root powder was analyzed under different conditions, as shown in Fig. 22. Temperature is an essential parameter for adsorption studies that affect

Table 3
Pseudo-first-order kinetic constants for azo dyes uptake by the adsorbent

Type of azo dye	Azo dye solution's concentration in mg·L^{-1}	Pseudo-first-order constants		Regression values (R^2)
		K (min^{-1})	Calculated q_e (mg·g^{-1})	
RO-16	25	0.0668	11.492	0.918
	50	0.0736	28.504	0.921
	75	0.0760	46.559	0.927
	100	0.0829	83.716	0.946
	125	0.0714	84.139	0.936
	150	0.0692	84.725	0.927
RR-120	25	0.0678	12.445	0.927
	50	0.0714	29.040	0.911
	75	0.0737	54.935	0.928
	100	0.0875	84.121	0.924
	125	0.0921	94.189	0.931
	150	0.0985	132.573	0.943
RB-19	25	0.0645	11.561	0.916
	50	0.0737	30.794	0.922
	75	0.0898	69.343	0.935
	100	0.0806	74.989	0.930
	125	0.0875	92.336	0.935
	150	0.0936	115.88	0.942

Table 4
Pseudo-second-order kinetic constants for azo dyes uptake by *Prosopis juliflora* roots activated charcoal

Type of azo dye	Azo dye solution's concentration in mg·L^{-1}	K (10^{-3}) g·mg^{-1}·min^{-1}	Calculated q_e (mg·g^{-1})	h (mg·g^{-1}·min^{-1})	Expected q_e (mg·g^{-1})	Regression values (R^2)
RO-16	25	8.980	13.988	1.751	12.983	0.997
	50	4.722	26.878	3.607	25.126	0.997
	75	2.826	41.766	3.986	38.214	0.996
	100	1.969	56.552	4.552	50.873	0.995
	125	1.353	66.763	4.793	59.129	0.994
	150	1.114	72.361	5.216	68.427	0.994
RR-120	25	7.763	13.968	1.522	12.840	0.997
	50	3.600	26.513	2.778	24.450	0.997
	75	2.870	38.642	3.623	36.892	0.979
	100	1.530	51.235	4.617	48.711	0.969
	125	0.949	62.458	4.655	59.122	0.994
	150	0.782	72.357	4.925	68.458	0.994
RB-19	25	8.186	13.514	1.495	12.631	0.975
	50	4.250	25.641	2.466	24.221	0.976
	75	2.522	37.307	3.640	35.015	0.964
	100	1.478	52.363	4.908	47,234	0.965
	125	1.258	66.672	5.392	59.286	0.972
	150	1.009	73.314	4.484	67.194	0.964

the adsorption process. Referring to the temperature study plots (Fig. 22), the maximum amount of azo dye removal was attained at 20°C. When the temperature was increased gradually up to 60°C, the sudden decrement of azo dye uptake by the *P. juliflora* root powder was noticed. Because

of the exothermic nature of the adsorption process, due to the decreases in the size of the adsorbent surface, the dyes received by the *P. juliflora* root powder were reduced [68]. Fig. 23 shows the adsorption process's thermodynamic plots (logK_c vs. $1/T$) in various azo dye concentrations from 25 to

Table 5
Thermodynamic constants for azo dyes uptake using *Prosopis juliflora* roots activated charcoal

RO-16 concentration (initial) in mg·L^{-1}	Enthalpy ($\Delta H°$) kJ·mol^{-1}	Entropy ($\Delta S°$) J·mol^{-1}	Gibbs energy ($\Delta G°$) kJ·mol^{-1}			
			15°C	30°C	45°C	60°C
25	73.519	196.024	−13.106	−9.580	−8.362	−7.472
50	41.822	101.345	−9.856	−8.532	−7.649	−6.328
75	24.825	51.552	−7.362	−6.338	−6.037	−5.824
100	17.564	34.824	−6.125	−5.832	−5.015	−4.923
125	14.724	31.283	−5.724	−5.245	−4.992	−4.325
150	12.271	27.834	−4.762	−4.524	−4.327	−4.081
RR-120 concentration (initial) in mg·L^{-1}						
25	45.434	113.234	−11.298	−9.438	−8.834	−6.683
50	31.298	75.582	−9.462	−7.736	−7.336	−6.026
75	18.362	37.725	−8.642	−6.224	−5.906	−5.124
100	15.182	31.923	−6.766	−5.835	−5.215	−4.853
125	12.837	24.846	−5.833	−5.053	−4.723	−4.257
150	10.699	19.274	−5.032	−4.636	−4.224	−4.003
RB-19 concentration (initial) in mg·L^{-1}						
25	34.623	80.832	−9.102	−7.792	−7.068	−6.491
50	21.392	42.292	−8.432	−6.923	−6.226	−5.345
75	18.696	37.143	−6.692	−5.724	−5.162	−4.346
100	12.823	26.882	−6.078	−5.026	−4.622	−4.028
125	11.180	22.174	−5.121	−4.224	−4.098	−3.946
150	9.984	19.924	−4.446	−4.012	−3.925	−3.281

Table 6
Desorption of azo dyes from the spent *Prosopis juliflora* roots activated charcoal

Initial concentration (25 mg·L^{-1})	Recovery of azo dyes (%)	Concentration of H$_2$SO$_4$			
		0.10 N	0.20 N	0.30 N	0.40 N
		% Desorption of azo dyes			
RO-16	98.25	89.26	93.57	93.82	91.31
RR-120	87.72	80.93	83.25	83.94	81.84
RB-19	81.18	71.73	74.58	75.23	73.83

150 mg·L^{-1}. Referring to the thermodynamic plots, the slope and intercept values ($\Delta H°$ and $\Delta S°$) were calculated and represented in Table 5. Due to the spontaneous nature of the prepared adsorbent material, the values of $\Delta G°$ become negative with positive $\Delta H°$ values, and it confirms the endothermic nature of the adsorption process. The positive values of $\Delta S°$ confirm the uncertainty of the interface between solid and liquid and its increases during the adsorption process in the aqueous medium [61].

3.16. Desorption studies

The desorption process is directly proportional to the spent adsorbent and its ability to desorb the dyes from the aqueous medium. The desorption studies using concentrated sulfuric acid (0.1–0.4 N) for the recovery of azo dyes have been carried out in Table 6. It was identified that the maximum amount of azo dye recovery was achieved when the sulfuric acid concentration was very high. The recovery of dyes gets increased by increasing the concentration of sulfuric acid up to 0.3 N, and after that, it attains a constant rate [69]. No increase in dye recovery was found when the concentration of sulfuric acid was increased. Hence, the optimum level of dyes recovery using sulfuric acid is fixed at 0.3 N, and the spent adsorbent was recovered and used for further adsorption studies.

To confirm the method of adsorption using *P. juliflora* powder, the system needs to be benchmarked with the other

Table 7
List of research work conducted for azo dyes removal using *Prosopis juliflora* roots activated charcoal

Type of azo dyes	Adsorption efficiency	Concentration of azo dye solutions (mg·L^{-1})	Optimum pH	Adsorbent dose	Contact time (min)	Reference
RO-16, RR-120 and RB-19	99.6%, 94.43% and 82.26%	25	2.0	2 g·L^{-1}	50	In this study
DY-12	85%	100	3.0	450 mg	90	[70]
DR-23	109.89 mg·g^{-1}	75	3.0	100 mg	30	[66]
MG	50 mg·g^{-1}	50	7.0	50 mg/50 mL	50	[71]
AB	98.2%	60	6.0	1 g	60	[72]
DBMR	91.8%	50	2.0	100 mg	10	[18]
Gold HE-R and green HE-4BD	50 and 62.50 mg·g^{-1}	25	1.0	2 g·L^{-1}	60	[73]

azo dye adsorption process or systems. Table 7 represents the comparison of adsorption of various dyes and metal ions with this adsorption process to evaluate the performance of prepared chemically activated *P. juliflora* root charcoal.

4. Conclusion

A batch adsorption study investigated the removal of azo dyes from the aqueous medium using activated *P. juliflora* root powder. The findings of this investigative work were concluded as follows:

- A high amount of azo dyes uptake from the prepared synthetic solutions was achieved at the pH of 2.0 within 50 min of contact time, using 2 g·L^{-1} of *P. juliflora* root powder adsorbent and a dye concentration of 25 mg·L^{-1}.
- The ideal temperature level for the entire batch study was found to be 30°C.
- The Langmuir, Freundlich and R-P isotherm studies fitted well with the adsorption process.
- Pseudo-first-order and pseudo-second-order kinetic studies confirmed the high regression fit with the adsorption process.
- The juliflora root powder activated carbon adsorbs 99.6% of RO-16, 94.43% of RR-120, and 82.26% of RB-19 azo dyes.
- The maximum recovery of azo dyes was achieved by adding 0.3 N of sulphuric acid to the spent adsorbent.

References

[1] J. Oliver Paul Nayagam, K. Prasanna, Utilization of shell-based agricultural waste adsorbents for removing dyes: a review, Chemosphere, 291 (2022) 132737, doi: 10.1016/j.chemosphere.2021.132737.

[2] S. Candamano, A. Policicchio, G. Conte, R. Abarca, C. Algieri, S. Chakraborty, S. Curcio, V. Calabrò, F. Crea, R.G. Agostino, Preparation of foamed and unfoamed geopolymer/NaX zeolite/activated carbon composites for CO_2 adsorption, J. Cleaner Prod., 330 (2022) 129843, doi: 10.1016/j.jclepro.2021.129843.

[3] S.B. Jadhav, S.M. Yedurkar, S.S. Phugare, J.P. Jadhav, Biodegradation studies on Acid Violet 19, a triphenylmethane dye, by *Pseudomonas aeruginosa* BCH, Clean – Soil, Air, Water, 40 (2012) 551–558.

[4] S.J. Cobbina, A.B. Duwiejuah, A.K. Quainoo, Single and simultaneous adsorption of heavy metals onto groundnut shell biochar produced under fast and slow pyrolysis, Int. J. Environ. Sci. Technol., 16 (2019) 3081–3090.

[5] X. Ma, Y. Liu, Q. Zhang, S. Sun, X. Zhou, Y. Xu, A novel natural lignocellulosic biosorbent of sunflower stem-pith for textile cationic dyes adsorption, J. Cleaner Prod., 331 (2022) 129878, doi: 10.1016/j.jclepro.2021.129878.

[6] X. Liu, J. Tian, Y. Li, N. Sun, S. Mi, Y. Xie, Z. Chen, Enhanced dyes adsorption from wastewater via Fe_3O_4 nanoparticles functionalized activated carbon, Colloids Surf., A, 561 (2019) 388–394.

[7] A. Witek-Krowiak, R.G. Szafran, S. Modelski, Biosorption of heavy metals from aqueous solutions onto peanut shell as a low-cost biosorbent, Desalination, 265 (2011) 126–134.

[8] A. Mittal, J. Mittal, Chapter 11 – Hen Feather: A Remarkable Adsorbent for Dye Removal, S.K. Sharma, Ed., Green Chemistry for Dyes Removal from Wastewater, Scrivener Publishing LLC, USA, 2015, pp. 409–457.

[9] A. Mariyam, J. Mittal, F. Sakina, R.T. Baker, A.K. Sharma, A. Mittal, Efficient batch and fixed-bed sequestration of a basic dye using a novel variant of ordered mesoporous carbon as adsorbent, Arabian J. Chem., 14 (2021) 103186, doi: 10.1016/j.arabjc.2021.103186.

[10] C. Arora, S. Soni, P.K. Bajpai, J. Mittal, A. Mariyam, Dye Removal from Waste Water Using Metal Organic Frameworks, 26th ed., Elsevier Inc., UK, 2021.

[11] V. Kumar, P. Saharan, A.K. Sharma, A. Umar, I. Kaushal, A. Mittal, Y. Al-Hadeethi, B. Rashad, Silver doped manganese oxide-carbon nanotube nanocomposite for enhanced dye-sequestration: isotherm studies and RSM modelling approach, Ceram. Int., 46 (2020) 10309–10319.

[12] R.T. Prabha, Dr. Udayashankara T.H., Removal of heavy metal from synthetic wastewater using rice husk and groundnut shell as adsorbents, IOSR J. Environ. Sci. Toxicol. Food Technol. (IOSR-JESTFT), 8 (2014) 26–34.

[13] H. Boubaker, R.B. Arfi, K. Mougin, C. Vaulot, S. Hajjar, P. Kunneman, G. Schrodj, A. Ghorbal, New optimization approach for successive cationic and anionic dyes uptake using reed-based beads, J. Cleaner Prod., 307 (2021) 127218, doi: 10.1016/j.jclepro.2021.127218.

[14] E.M. Sahin, T. Tongur, E. Ayranci, Removal of azo dyes from aqueous solutions by adsorption and electrosorption as

monitored with in-situ UV-visible spectroscopy, Sep. Sci. Technol., 55 (2020) 3287–3298.

[15] X.-K. Ouyang, L.-P. Yang, Z.-S. Wen, Adsorption of Pb(II) from solution using peanut shell as biosorbent in the presence of amino acid and sodium chloride, BioResources, 9 (2014) 2446–2458.

[16] U. Kumari, A. Mishra, H. Siddiqi, B.C. Meikap, Effective defluoridation of industrial wastewater by using acid modified alumina in fixed-bed adsorption column: experimental and breakthrough curves analysis, J. Cleaner Prod., 279 (2021) 123645, doi: 10.1016/j.jclepro.2020.123645.

[17] J. Lehmann, J.P. da Silva Jr., C. Steiner, T. Nehls, W. Zech, B. Glaser, Nutrient availability and leaching in an archaeological Anthrosol and a Ferralsol of the Central Amazon basin: fertilizer, manure and charcoal amendments, Plant Soil, 249 (2003) 343–357.

[18] M.K. Raman, G. Muthuraman, Removal of binary mixture of textile dyes on *Prosopis juliflora* pods – equilibrium, kinetics and thermodynamics studies, Iran. J. Energy Environ., 8 (2017) 48–55.

[19] V.E. Vallejo, Z. Arbeli, W. Terán, N. Lorenz, R.P. Dick, F. Roldan, Effect of land management and *Prosopis juliflora* (Sw.) DC trees on soil microbial community and enzymatic activities in intensive silvopastoral systems of Colombia, Agric. Ecosyst. Environ.,150 (2012) 139–148.

[20] N. Yousif, Textile industry wastewaters treatment, J. Phys. Ther. Sci., 9 (2018) 1–11.

[21] R. Shan, Y. Shi, J. Gu, Y. Wang, H. Yuan, Single and competitive adsorption affinity of heavy metals toward peanut shell-derived biochar and its mechanisms in aqueous systems, Chin. J. Chem. Eng., 28 (2020) 1375–1383.

[22] S. Idris, Y.A. Iyaka, B.E.N. Dauda, M.M. Ndamitso, M.T. Umar, Kinetic study of utilizing groundnut shell as an adsorbent in removing chromium and nickel from dye effluent, Am. Chem. Sci. J., 2 (2012) 12–24.

[23] H. Karimi-Maleh, A. Ayati, R. Davoodi, B. Tanhaei, F. Karimi, S. Malekmohammadi, Y. Orooji, L. Fu, M. Sillanpää, Recent advances in using of chitosan-based adsorbents for removal of pharmaceutical contaminants: a review, J. Cleaner Prod., 291 (2021) 125880, doi: 10.1016/j.jclepro.2021.125880.

[24] R. Arora, Adsorption of heavy metals–a review, Mater. Today Proc.,18 (2019) 4745–4750.

[25] Qurrat-ul-Ain, S. Khurshid, Z. Gul, J. Khatoon, M.R. Shah, I. Hamid, I.A.T. Khan, F. Aslam, Anionic azo dyes removal from water using amine-functionalized cobalt–iron oxide nanoparticles: a comparative time-dependent study and structural optimization towards the removal mechanism, RSC Adv., 10 (2019) 1021–1041.

[26] L. Xia, S. Zhou, C. Zhang, Z. Fu, A. Wang, Q. Zhang, Y. Wang, X. Liu, X. Wang, W. Xu, Environment-friendly *Juncus effusus*-based adsorbent with a three-dimensional network structure for highly efficient removal of dyes from wastewater, J. Cleaner Prod., 259 (2020) 120812, doi: 10.1016/j.jclepro.2020.120812.

[27] N.A.A. Qasem, R.H. Mohammed, D.U. Lawal, Removal of heavy metal ions from wastewater: a comprehensive and critical review, npj Clean Water, 4 (2021) 36, doi: 10.1038/s41545-021-00127-0.

[28] A.A. Alqadami, Mu. Naushad, M.A. Abdalla, T. Ahamad, Z.A. ALOthman, S.M. Alshehri, A.A. Ghfar, Efficient removal of toxic metal ions from wastewater using a recyclable nanocomposite: a study of adsorption parameters and interaction mechanism, J. Cleaner Prod., 156 (2017) 426–436.

[29] S. Chakraborty, A. Mukherjee, S. Das, N.R. Maddela, S. Iram, P. Das, Study on isotherm, kinetics, and thermodynamics of adsorption of crystal violet dye by calcium oxide modified fly ash, Environ. Eng. Res., 26 (2021) 190372, doi: 10.4491/eer.2019.372.

[30] M. Kabir, S. Singh, M.J. Ferrantino, The Textile-Clothing Value Chain in India and Bangladesh: How Appropriate Policies Can Promote (or Inhibit) Trade and Investment, Policy Research Working Paper; No. 8731. World Bank, Washington, D.C., World Bank, 2019. Available at: https://openknowledge.worldbank.org/handle/10986/31263 License: CC BY 3.0 IGO

[31] A. Daochalermwong, N. Chanka, K. Songsrirote, P. Dittanet, C. Niamnuy, A. Seubsai, Removal of heavy metal ions using modified celluloses prepared from pineapple leaf fiber, ACS Omega, 5 (2020) 5285–5296.

[32] V. Kromah, G. Zhang, Aqueous adsorption of heavy metals on metal sulfide nanomaterials: synthesis and application, Water (Switzerland), 13 (2021) 1843, doi: 10.3390/w13131843.

[33] S.A. Olawale, A. Bonilla-Petriciolet, D.I. Mendoza-Castillo, C.C. Okafor, L. Sellaoui, M. Badawi, Thermodynamics and mechanism of the adsorption of heavy metal ions on keratin biomasses for wastewater detoxification, Adsorpt. Sci. Technol., 2022 (2022) 7384924, doi: 10.1155/2022/7384924.

[34] Y. Qin, M. Yuan, Y. Hu, Y. Lu, W. Lin, Y. Ma, X. Lin, T. Wang, Preparation and interaction mechanism of nano disperse dye using hydroxypropyl sulfonated lignin, Surf. Coat. Technol., 152 (2020) 280–287.

[35] A. Kaur, S. Sharma, Removal of heavy metals from waste water by using various adsorbents – a review, Indian J. Sci. Technol., 10 (2017) 117269, doi: 10.17485/ijst/2017/v10i34/117269.

[36] F. Elmi, F. Mohammadi Damghani, M. Shokrollahzadeh Taleshi, Kinetic and isotherm studies of adsorption of the metribuzin herbicide on an Fe_3O_4/CNT@PDA hybrid magnetic nanocomposite in wastewater, Ind. Eng. Chem. Res., 59 (2020) 9604–9610.

[37] S.R. Mishra, R. Chandra, J. Kaila A., S. Darshi B., Kinetics and isotherm studies for the adsorption of metal ions onto two soil types, Environ. Technol. Innovation, 7 (2017) 87–101.

[38] F. Kanwal, R. Rehman, I.Q. Bakhsh, Batch wise sorptive amputation of diamond green dye from aqueous medium by novel polyaniline-*Alstonia scholaris* leaves composite in ecofriendly way, J. Cleaner Prod., 196 (2018) 350–357.

[39] S. Sivakumar, P. Muthirulan, M. Meenakshi Sundaram, Adsorption kinetic and isotherm studies of Azure A on various activated carbons derived from agricultural wastes, Arabian J. Chem., 12 (2019) 1507–1514.

[40] F. Batool, J. Akbar, S. Iqbal, S. Noreen, S.N.A. Bukhari, Study of isothermal, kinetic, and thermodynamic parameters for adsorption of cadmium: an overview of linear and nonlinear approach and error analysis, Bioinorg. Chem. Appl., 2018 (2018) 3463724, doi: 10.1155/2018/3463724.

[41] S. Mehdi Niknam, M. Kashaninejad, I. Escudero, M. Teresa Sanz, S. Beltrán, J.M. Benito, Valorization of olive mill solid residue through ultrasound-assisted extraction and phenolics recovery by adsorption process, J. Cleaner Prod., 316 (2021) 128340, doi: 10.1016/j.jclepro.2021.128340.

[42] U.A. Edet, A.O. Ifelebuegu, Kinetics, isotherms, and thermodynamic modeling of the adsorption of phosphates from model wastewater using recycled brick waste, Processes, 8 (2020) 665, doi: 10.3390/pr8060665.

[43] J. Sheeja, K. Sampath, R. Kesavasamy, Experimental investigations on adsorption of reactive toxic dyes using hedyotis umbellate activated carbon, Adsorpt. Sci. Technol., 2021 (2021) 5035539, doi: 10.1155/2021/5035539.

[44] A.O. Dada, F.A. Adekola, E.O. Odebunmi, A.S. Ogunlaja, O.S. Bello, Two–three parameters isotherm modeling, kinetics with statistical validity, desorption and thermodynamic studies of adsorption of Cu(II) ions onto zerovalent iron nanoparticles, Sci. Rep., 11 (2021) 16454, doi: 10.1038/s41598-021-95090-8.

[45] K.S. Obayomi, M. Auta, A.S. Kovo, Isotherm, kinetic and thermodynamic studies for adsorption of lead(II) onto modified Aloji clay, Desal. Water Treat., 181 (2020) 376–384.

[46] N.K. Haro, I.V.J. Dávila, K.G.P. Nunes, M.A.E. de Franco, N.R. Marcilio, L.A. Féris, Kinetic, equilibrium and thermodynamic studies of the adsorption of paracetamol in activated carbon in batch model and fixed-bed column, Appl. Water Sci., 11 (2021) 38, doi: 10.1007/s13201-020-01346-5.

[47] M. Hosseinzehi, M. Khatebasreh, A. Dalvand, Modeling of Reactive Black 5 azo dye adsorption from aqueous solution on activated carbon prepared from poplar sawdust using response surface methodology, Int. J. Environ. Anal. Chem., 102 (2022) 6970–6987.

[48] W. Mwandira, K. Nakashima, S. Kawasaki, A. Arabelo, K. Banda, I. Nyambe, M. Chirwa, M. Ito, T. Sato, T. Igarashi, H. Nakata, S. Nakayama, M. Ishizuka, Biosorption of Pb(II) and Zn(II) from aqueous solution by *Oceanobacillus profundus* isolated from an abandoned mine, Sci. Rep., 10 (2020) 21189, doi: 10.1038/s41598-020-78187-4.

[49] W. Kaminski, E. Tomczak, P. Tosik, Kinetics of azo dyes sorption onto low-cost sorbents, Desal. Water Treat., 55 (2015) 2675–2679.

[50] M. Priyanka, M.P. Saravanakumar, Ultrahigh adsorption capacity of starch derived zinc based carbon foam for adsorption of toxic dyes and its preliminary investigation on oil-water separation, J. Cleaner Prod., 197 (2018) 511–524.

[51] H.N. Tran, E.C. Lima, R.-S. Juang, J.-C. Bollinger, H.-P. Chao, Thermodynamic parameters of liquid–phase adsorption process calculated from different equilibrium constants related to adsorption isotherms: a comparison study, J. Environ. Chem. Eng., 9 (2021) 106674, doi: 10.1016/j.jece.2021.106674.

[52] N.G. Rincón-Silva, J.C. Moreno-Piraján, L.G. Giraldo, Thermo-dynamic study of adsorption of phenol, 4-chlorophenol, and 4-nitrophenol on activated carbon obtained from eucalyptus seed, J. Chem., 2015 (2015) 569403, doi: 10.1155/2015/569403.

[53] L. Panda, S.K. Jena, S.S. Rath, P.K. Misra, Heavy metal removal from water by adsorption using a low-cost geopolymer, Environ. Sci. Pollut. Res., 27 (2020) 24284–24298.

[54] Y. Venkatraman, A.K. Priya, Removal of heavy metal ion con-centrations from the wastewater using tobacco leaves coated with iron oxide nanoparticles, Int. J. Environ. Sci. Technol., 19 (2022) 2721–2736.

[55] M.Z.A. Zaimee, M.S. Sarjadi, Md L. Rahman, Heavy metals removal from water by efficient adsorbents, Water (Switzerland), 13 (2021) 2659, doi: 10.3390/w13192659.

[56] R.J. Nathan, C.E. Martin, D. Barr, R.J. Rosengren, Simultaneous removal of heavy metals from drinking water by banana, orange and potato peel beads: a study of biosorption kinetics, Appl. Water Sci., 11 (2021) 116, doi: 10.1007/s13201-021-01457-7.

[57] L. Su, H. Zhang, K. Oh, N. Liu, Y. Luo, H. Cheng, G. Zhang, X. He, Activated biochar derived from spent *Auricularia auricula* substrate for the efficient adsorption of cationic azo dyes from single and binary adsorptive systems, Water Sci. Technol., 84 (2021) 101–121.

[58] P. Phuengphai, T. Singjanusong, N. Kheangkhun, A. Wattana-kornsiri, Removal of copper(II) from aqueous solution using chemically modified fruit peels as efficient low-cost biosorbents, Water Sci. Eng., 14 (2021) 286–294.

[59] F.O. Afolabi, P. Musonge, B.F. Bakare, Evaluation of lead(II) removal from wastewater using banana peels: optimization study, Pol. J. Environ. Stud., 30 (2021) 1487–1496.

[60] W. El Malti, A. Hijazi, Z.A. Khalil, Z. Yaghi, M.K. Medlej, M. Reda, Comparative study of the elimination of copper, cadmium, and methylene blue from water by adsorption on the citrus *Sinensis* peel and its activated carbon, RSC Adv., 12 (2022) 10186–10197.

[61] D.L. Gómez-Aguilar, J.P. Rodríguez-Miranda, O.J. Salcedo-Parra, Fruit peels as a sustainable waste for the biosorption of heavy metals in wastewater: a review, Molecules, 27 (2022) 2124, doi: 10.3390/molecules27072124.

[62] B.N. Pham, J.-K. Kang, C.-G. Lee, S.-J. Park, Removal of heavy metals (Cd^{2+}, Cu^{2+}, Ni^{2+}, Pb^{2+}) from aqueous solution using *Hizikia fusiformis* as an algae-based bioadsorbent, Appl. Sci., 11 (2021) 8604, doi: 10.3390/app11188604.

[63] M. Becker, M. Alvarez, G. Heller, P. Leparmarai, D. Maina, I. Malombe, M. Bollig, H. Vehrs, Land-use changes and the invasion dynamics of shrubs in Baringo, J. East. Afr. Stud., 10 (2016) 111–129.

[64] S.O. Owalude, A.C. Tella, Removal of hexavalent chromium from aqueous solutions by adsorption on modified groundnut hull, Beni-Suef Univ. J. Basic Appl. Sci., 5 (2016) 377–388.

[65] P.K. Obulapuram, T. Arfin, F. Mohammad, S.K. Khiste, M. Chavali, Studies towards the removal of Reactive Orange 16 dye, Polymers (Basel), I (2021) 1–16.

[66] N. Gopal, M. Asaithambi, P. Sivakumar, V. Sivakumar, Adsorption studies of a direct dye using polyaniline coated activated carbon prepared from *Prosopis juliflora*, J. Water Process Eng., 2 (2014) 87–95.

[67] S. Agarwal, V.K. Gupta, M. Ghasemi, J. Azimi-Amin, *Peganum harmala*-L seeds adsorbent for the rapid removal of noxious brilliant green dyes from aqueous phase, J. Mol. Liq., 231 (2017) 296–305.

[68] K.D. Belaid, S. Kacha, M. Kameche, Z. Derriche, Adsorption kinetics of some textile dyes onto granular activated carbon, J. Environ. Chem. Eng., 1 (2013) 496–503.

[69] C. Tejada-Tovar, Á. Villabona-Ortíz, Á.D. Gonzalez-Delgado, Adsorption of azo-anionic dyes in a solution using modified coconut (*Cocos nucifera*) mesocarp: kinetic and equilibrium study, Water (Switzerland), 13 (2021) 1382, doi: 10.3390/w13101382.

[70] L.K. Sanghavi, DR. Shashi V. Ranga, Study of operating parameters for removal of Direct Yellow 12 dye using *Prosopis juliflora* bark, Int. J. Res. Anal. Rev. (IJRAR), 6 (2019) 869–880.

[71] M. Thilagavathi, S. Arivoli, V. Vijayakumaran, Adsorption of malachite green from waste water using *Prosopis juliflora* bark carbon, Kuwait J. Sci., 42 (2015) 120–133.

[72] M. Kumar, R. Tamilarasan, Modeling studies: adsorption of aniline blue by using *Prosopis juliflora* carbon/Ca/alginate polymer composite beads, Carbohydr. Polym., 92 (2013) 2171–2180.

[73] Y. Zhang, G. Huang, C. An, X. Xin, X. Liu, M. Raman, Y. Yao, W. Wang, M. Doble, Transport of anionic azo dyes from aqueous solution to gemini surfactant-modified wheat bran: synchrotron infrared, molecular interaction and adsorption studies, Sci. Total Environ., 595 (2017) 723–732.